1981ApJS...47..117B

THE ASTROPHYSICAL JOURNAL SUPPLEMENT SERIES, 47: 117–138, 1981 October
© 1981. The American Astronomical Society. All rights reserved. Printed in U.S.A.

EMISSION LINE SPECTRA OF HERBIG-HARO OBJECTS

E. W. BRUGEL,[1] K. H. BÖHM,[2] AND E. MANNERY[2]
Astronomy Department, University of Washington
Received 1981 January 30; accepted 1981 April 6

ABSTRACT

Spectrophotometric data have been obtained for 12 Herbig-Haro nebulae with the multichannel spectrometer on the Mt. Palomar 5.08 m telescope and with the image intensified dissector scanner on the Kitt Peak 2.13 m telescope. Optical emission line fluxes are presented for the following Herbig-Haro objects: H-H 1 (NW), H-H 1 (SE), H-H 2A, H-H 2G, H-H 2H, H-H 3, H-H 7, H-H 11, H-H 24A, H-H 30, H-H 32, and H-H 40. Values for the electron temperature and electron density have been determined for 10 of these condensations. Significant inhomogenities in the line-forming regions of these H-H objects are indicated by the derived N_e-T_e diagrams. Empirical two-component density models have been constructed to interpret the emission line spectra of the five brightest condensations. Slightly less satisfactory homogeneous models are presented for the remaining five objects.

With the aid of these models, ionic abundances for O I, O II, O III, N I, N II, S II, S III, Ca II, Ne III, C I, and Mg I have been determined. In all observed nebulae, these abundances are consistent with "cosmic" Population I elemental abundances. In addition, iron abundances based upon the [Fe II] and [Fe III] lines have been ascertained for the first time, and these results are also indicative of a Population I abundance.

Gas phase depletions in the refractory elements might be expected for objects located in regions of recent star formation in which there are large concentrations of dust. However, there is no evidence for enhanced dust formation inside any Herbig-Haro object, as illustrated by the derived normal "cosmic" abundances of Ca and Fe.

The emission line variability in H-H 1 and H-H 2H is investigated.

Subject headings: stars: abundances — stars: emission-line — stars: formation — stars: pre–main-sequence

I. INTRODUCTION

An universally accepted *complete* description of the physical conditions within Herbig-Haro (H-H) objects is presently unavailable in spite of some impressive results of the shock wave interpretation (Schwartz 1975) of their line spectra. The accumulation of considerable empirical data during the past decade has significantly increased our knowledge of H-H objects while also exhibiting more clearly some of the enigmatic characteristics of this class of nebulae.

A major recent advance in the interpretation of the emission line spectra of H-H objects has been the development of detailed shock models (Raymond 1976, 1979; Dopita 1978*b*). Although these models produce fairly good quantitative agreement for some H-H objects, there are other objects, such as H-H 47 (Dopita 1978*b*), H-H 7, and H-H 11 (Böhm, Brugel, and Mannery 1980), which cannot yet be explained in this way. However, these discrepancies may be technical rather than fundamental in nature.

Additionally, recent ultraviolet observations of H-H 1 (Ortolani and d'Odorico 1980; Böhm, Böhm-Vitense, and Brugel 1981) present added difficulties for the simple shock wave interpretation. Specifically, it is not possible to explain the visible (Böhm, Siegmund, and Schwartz 1976; Schwartz 1976; Dopita 1978*a*) and the ultraviolet line spectrum by the same shock wave model.

These facts show that considerable improvements of the theory are needed before shock models can be successfully applied to describe the detailed observed line spectra of all H-H objects over all spectral regions. In the meantime, we believe that spectrophotometric studies of the emission line spectra will continue to play an important role in the investigation of these objects. In particular, the optical line spectra contain sufficient information for constructing "empirical" models, for ascertaining the physical parameters electron tempera-

[1]Visiting Astronomer at the Kitt Peak National Observatory, which is operated by the Association of Universities for Research in Astronomy, Inc., under contract with the National Science Foundation.

[2]Guest Investigator at the Hale Observatories, which were jointly operated by the Carnegie Institution of Washington and the California Institute of Technology.

© American Astronomical Society • Provided by the NASA Astrophysics Data System

1981ApJS...47..117B

ture, electron density, degree of ionization, and filling factors, and for determining the chemical composition. This heuristic interpretation will have to be replaced by more sophisticated shock wave models as soon as they become available. Spectrophotometric investigations may also provide information pertaining to the relationship between brightness changes and variations in these physical parameters. Preliminary attempts to quantify the variability of these parameters were made by Böhm, Perry, and Schwartz (1973) and Böhm and Brugel (1979).

In this study we shall present and interpret the emission line spectra for H-H 1 (NW), H-H 1 (SE), H-H 2A, H-H 2G, H-H 2H, H-H 3, H-H 7, H-H 11, H-H 24A, H-H 30, H-H 32, and H-H 40 (see the catalog of Herbig 1974). Some of these objects (viz., H-H 1, H-H 2H, H-H 2G, and H-H 3, H-H 24A, H-H 32, and H-H 40) have also been studied by Dopita (1978*b*) using different instruments. However, our MCSP observations cover a considerably wider wavelength range ($3200<\lambda<11000$ Å) permitting the study of near infrared lines. Of particular interest are the [S II] lines $\lambda\lambda$10317 and 10336 which are used (in combination with the [S II] $\lambda\lambda$4068/4076 lines) for a reliable determination of the reddening (Miller 1968; Böhm, Schwartz, and Siegmund 1974).

Our data for H-H 1 (NW) and H-H 2H will be discussed in relationship to previous spectrophotometric observations (Böhm 1956; Böhm, Perry, and Schwartz 1976; Böhm and Brugel 1979). In addition, we shall also attempt to derive detailed descriptions of the physical conditions within the individual nebulae.

II. OBSERVATIONS

The spectrophotometric data used in this study are based upon observations obtained with the multichannel spectrometer (MSCP II; Oke 1969) on the 5.08 m telescope during the period 1978 Sep 22–25. Additional observations were acquired with the image intensified dissector scanner (IIDS) on the 2.13 m telescope at Kitt Peak National Observatory during 1978 Nov 25–28. These observations have been described in detail in an earlier paper (Brugel, Böhm, and Mannery 1981; hereafter Paper I) where they were used to investigate the continuum of H-H objects.

A typical MCSP scan consisted of 279 different wavelength intervals each with a bandwidth of 20 Å, although in some cases more or fewer grating settings have been used (see Table 1). The preselected wavelength settings were chosen to permit observations of all important "known" emission lines in the wavelength range 3144–11,000 Å. It is possible, although not probable, that some relatively strong lines have not been detected since the whole spectrum has not been covered. The specific number of spectral scans, the aperture sizes, and integration times per grating setting are listed in Table 1.

Because of the relatively wide bandwidth of the MCSP data (20 Å), the line flux measurements must be corrected for the continuum contributions to the observed flux. This is accomplished by subtracting out the continuum determined in Paper I. Since the continua are extremely weak, these corrections are small for the moderately strong lines. However, the continuum does become an appreciable fraction of the line emission for the weaker lines, particularly for those in the blue. The continua are not detected in H-H 1 (SE), H-H 3, H-H 7, and H-H 11, and thus the corrections could not be applied to these objects.

Table 2 lists the observed and reddening corrected relative line fluxes (with $H\beta=100$) for all the MCSP II observations (see § III for reddening determinations). These line intensities are corrected for continuum contamination whenever possible. The absolute flux of any line can be obtained from the appropriate $H\beta$ flux given in Table 3. For any object with more than one spectral scan, the line intensities presented in Tables 2 and 3 represent weighted means. The weighting parameter is simply the inverse standard deviation due to the photon statistics.

TABLE 1

MULTICHANNEL SPECTROMETER (MCSP II) OBSERVATIONS OF HERBIG-HARO OBJECTS

Object	Number of Observations	Aperture (arc seconds)	Number of Wavelengths	Integration Time
H-H 1 (NW) ...	2	5.″0, 5.″0	279, 434	400, 500
H-H 1 (SE)	1	5.0	93	250
H-H 2A	2	3.6, 3.6	279, 279	600, 600
H-H 2G	1	5.0	279	400
H-H 2H	1	5.0	279	400
H-H 3	1	3.6	155	400
H-H 7	1	7.0	217	800
H-H 11	1	5.0	279	800
H-H 32	3	7.0, 5.0, 5.0	248, 279, 372	600, 400, 400

NOTE.—The integration time is given in seconds per grating setting (see text).

© American Astronomical Society • Provided by the NASA Astrophysics Data System

1981ApJS...47..117B

TABLE 2A

OBSERVED (F) AND REDDENING-CORRECTED (F) RELATIVE EMISSION LINE FLUXES FOR HERBIG-HARO OBJECTS OBSERVED WITH MCSP

Ion	Line (A)	H-H 1 (NW) F	H-H 1 (NW) F_o	H-H 1 (SE) F	H-H 1 (SE) F_o	H-H 2A F	H-H 2A F_o	H-H 2G F	H-H 2G F_o	H-H 2H F	H-H 2H F_o
[OII]	3726/29	148.3	230.7	347.7	541.3	148.5	211.3	112.5	170.1	122.4	169.2
H12	3750	(1.6)	(2.5)	(13)	(20)	3.6	5.1	5.2	7.8	3.8	5.1
H11	3770	(1.1)	(1.8)			1.2	1.6	*	*	4.5	6.1
H10	3798	*	*	*	*	*	*	*	*	*	*
H9	3835	2.5	3.7	*	*	1.0	1.3	3.9	5.6	2.6	3.5
[NeIII]	3868	3.8	5.5	*	*	10.2	13.9	8.9	12.6	9.9	13.0
H8	3888	8.2	11.8	(22)	(32)	6.8	9.1	8.9	12.6	7.2	9.5
CaII	3933	13.2	18.6	*	*	7.0	9.3	13.5	18.7	11.2	14.4
CaII [NeIII] H7	3968	*	*	*	*	*	*	*	*	*	*
[SII]	4069/76	49.0	65.2	77.6	103.4	48.9	61.4	66.4	86.8	51.6	63.5
Hδ	4101	14.5	19.0	*	*	15.2	18.8	17.7	22.8	13.0	15.8
[FeII]	4114	*	*	*	*	*	*	*	*	*	*
[FeII]	4230	3.0	3.8	(13)	(17)	*	*	4.1	5.1	3.0	3.5
[FeII]	4244	4.8	6.0	(18)	(23)	*	*	*	*	*	*
[FeII]	4276	*	*	*	*	*	*	*	*	*	*
[FeII]	4287	*	*	*	*	*	*	*	*	*	*
[FeII]	4319	2.8	3.3	*	*	*		2.4	2.8	2.5	2.8
Hγ	4340	33.6	39.9	*	*	30.0	34.4	34.7	40.8	30.1	34.1
[FeII] [OIII]	4359 4369	7.7	9.1	(12)	(14)	6.6	7.5	2.7	3.1	4.8	5.5
[FeII]	4414/16	7.1	8.2	*	*	4.2	4.7	8.9	10.2	5.8	6.4
[FeII]	4452/58	3.6	4.1	*	*	*	*	1.5	1.7	4.0	4.5
He I	4471	1.1	1.3	*	*	*	*	1.8	2.0	1.4	1.5
Mg I	4571	4.9	5.4	*	*	2.3	2.5	5.2	5.7	3.6	3.9
[FeIII]	4658	3.0	3.2	*	*	8.3	8.8	5.1	5.4	6.3	6.5
HeII	4686	1.1	1.2	(7.7)	(8.1)			(1.0)	(1.0)	1.3	1.3
[FeII] [FeIII]	4728 4734	-	-	*	*	-	-	-	-	1.6	1.6
[FeII]	4815	3.0	3.0	*	*			3.5	4.5		
Hβ	4861	100.0	100.0	100.0	100.0	100.0	100.0	100.0	100.0	100.0	100.0
[FeII]	4889	1.6	1.6	*	*	*	*	6.2	6.2	3.2	3.2
[FeII]	4905	1.0	1.0	*	*	*	*				
[OIII]	4959	11.2	10.8	*	*	36.5	35.5	13.3	12.8	19.8	19.2
[OIII]	5007	49.4	44.8	70.8	64.2	117.6	108.9	39.3	35.9	67.5	62.9
[FeII]	5111	2.4	2.1	*	*			4.1	3.7	(1.2)	(1.1)
[FeII]	5158	24.3	21.2	14.2	12.4	4.4	4.0	6.0	5.3	*	*
[NI]	5200	16.2	13.9	83.2	71.1	12.5	11.0	25.5	22.0	11.0	9.8
[FeII]?	5220	1.1	0.9	*	*	-	-	2.7	2.3	-	-
[FeII] [FeIII]	5262/73 5270	11.1	9.2	*	*	8.8	7.6	20.6	17.3	11.6	10.1
[FeII]	5333	3.8	3.1	16.6	13.4	2.3	2.0	5.4	4.4	3.2	2.8
[FeII]	5376	1.6	1.3	*	*	1.4	1.2	3.0	2.4	1.5	1.3
[FeII]	5527	4.7	3.5	14.0	10.5	4.0	3.2	4.5	3.4	4.4	3.6
[OI]	5577	2.9	2.1	*	*			(1.7)	(1.3)	(0.9)	(0.7)
[NII]	5755	5.8	4.0	*	*	10.0	7.5	4.8	3.4	5.4	4.2
?	5864	2.9	1.9	*	*	-	-	2.9	2.0	1.4	1.0
[OI]	6300	202.0	122.4	*	*	164.2	110.2	238.7	149.4	175.7	122.0
[OI]	6363	57.5	34.3	*	*	30.0	19.9	61.0	37.6	31.5	21.6
[NII]	6548	84.1	48.1	*	*	*	*	*	*	*	*
Hα	6563	534.0	307.6	870.2	500.6	520.1	335.4	465.7	277.9	438.1	293.1
[NII]	6583	225.2	129.3	*	*	233.4	150.0	195.0	116.0	230.7	154.0
[SII]	6717	146.1	81.2	*	*	101.8	64.0	142.4	82.5	73.8	48.3
[SII]	6731	*	*	*	*	*	*	*	*	*	*
He I?	7065	3.8	2.0			4.5	2.7	-	-	-	-
[FeII]	7155	54.0	28.3	*	*	36.1	21.6	54.9	30.0	34.5	21.5
[FeII]	7172	19.6	10.2	*	*	16.8	10.0	17.9	9.7	12.9	8.0
[OII] [CaII] [OII]	7330	103.6	52.0	*	*	146.1	84.4	98.0	51.4	110.7	66.7
[FeII]?	7380	48.9	24.5	*	*	21.5	12.4	39.4	20.5	24.6	14.6
H(P) 9	8598	62.5	25.3	*	*	40.4	20.0	61.4	26.3	46.1	23.8
[FeII]	8617										
[SIII]	9069	(5.2)	(2.1)			*	*	*	*	*	*
[SIII]	9532	20.8	8.4	*	*	20.0	9.8	*	*	16.2	8.4

© American Astronomical Society • Provided by the NASA Astrophysics Data System

1981ApJS...47..117B

TABLE 2A—*Continued*

Ion	Line (A)	H-H 1 (NW) F	H-H 1 (NW) F_0	H-H 1 (SE) F	H-H 1 (SE) F_0	H-H 2A F	H-H 2A F_0	H-H 2G F	H-H 2G F_0	H-H 2H F	H-H 2H F_0
[CI]	9824	8.3	3.0	*	*	10.3	4.6	14.9	5.7	8.4	4.0
[CI]	9848	20.5	7.4	137.5	49.3	36.0	15.9	26.3	10.1	17.1	8.1
[SII]	10316	32.9	11.2	*	*	26.6	11.3	37.3	12.7	23.0	10.5
[SII]	10336	*	*	*	*	*	*	*	*	*	*
[NI]	10396	17.9	6.1	*	*	7.2	3.1	25.6	11.6	13.4	6.1
[NI]	10406	9.5	3.2	*	*	10.8	4.6	27.4	12.5	13.8	6.3
He I	10830	245.9	80.2	*	*	174.1	71.4	93.3	32.7	237.2	104.8

NOTE: An asterisk means that there was no grating setting for this wavelength. A dash means the line has not been detected. The usual normalization F (Hβ) = 100. has been used.

The integration times and wavelength coverage for IIDS data are presented in Table 4. The relative emission line intensities derived from these data were determined directly from graphically displayed spectra, F_λ versus wavelength. The total flux (in arbitrary units) in any given line is proportional to the area under the line profile. This area was calculated by assuming that the profile is approximately Gaussian in shape and then measuring three characteristic parameters (height at line center, *a*; height at width, *b*; width, *c*) which would define the Gaussian. The area (*A*) is then computed by the expression

$$A=\frac{ac}{2}\left[\pi/\ln\left(a/b\right)\right]^{1/2}, \qquad (1)$$

which represents the integrated area under the Gaussian. To test this technique several lines were measured with a planimeter; the results agreed to within 5%, which is less than the observational errors.

The relative line strengths (Hβ=100) derived from the IIDS data for H-H 1 (NW), H-H 2G, H-H 2H, H-H 3, H-H 11, H-H 24A, H-H 30, and H-H 40 are presented in Table 5. Both the observed and reddening corrected intensities are tabulated.

III. REDDENING CORRECTIONS

For all objects except H-H 24A and H-H 40, it was possible to utilize Miller's (1968) method to determine the amount of interstellar extinction. Since this has been discussed in detail in Paper I and in Böhm, Brugel, and Mannery (1980), our description will be brief. By comparing the theoretical intensity ratio of the transauroral (4069/4076 Å) to the auroral (10318/10336 Å) lines of [S II] with the measured ratio, we determine the interstellar extinction ratio in these two wavelengths. The Whitford-type reddening law derived by Schild (1977) was then used to find the extinction at the wavelength of the other observed lines.

Because of the lack of any better procedure, the following (admittedly somewhat questionable) approach was used for H-H 24A and H-H 40. By comparing the observed Balmer decrement to the theoretical recombination spectrum of hydrogen for Menzel's case (*b*), it is possible to determine the amount by which the relative intensities must be de-reddened.

This approach is problematic because it is known that the true Hα/Hβ ratios in H-H objects deviate considerably from Menzel's case (*b*) in some objects (Dopita 1978*b*; Böhm, Siegmund, and Schwartz 1976). However, for H-H 24A and H-H 40 the method gives values of $E(B-V)=0.71\pm0.2$ and 0.70 ± 0.2, respectively, which are compatible with the values of 0.92 and 0.71 obtained in yet another manner by Dopita (1978*b*). A summary of all the reddening determinations is given in Table 6.

IV. COMPARISON WITH DOPITA'S DATA

For those objects and wavelength regions for which Dopita (1978*b*) presents data the agreement is, in general, satisfactory but not outstanding. Line flux differences of up to 50% occur sometimes even for relatively strong lines. For H-H 32A, for which we have carried out especially long and repeated integrations, the deviations are even larger in the red part of the spectrum. Our observations do not show, for example, the very large Hα and [N II] λλ6548,6583 fluxes quoted by Dopita (1978*b*). In fact, for most of the objects we find smaller Hα/Hβ ratios than Dopita before the reddening correction is applied. Strangely, the often larger reddening corrections which are used by Dopita make the final fluxes similar to ours in a number of cases.

It should be noted that the determination of the reddening correction by Dopita (1978*b*) is much more indirect and uses more assumptions than the determination by Miller's (1968) method which we have used in most cases (see above). It obviously has to be considered as an accident that there seems to be better agreement between de-reddened than between original fluxes.

In some cases a part of the flux difference between Dopita's (1978*b*) and our measurements may be due to actual time changes occurring in the H-H object between 1976 (Dopita's observations) and 1978 (our observations). This argument may apply, for example, to H-H 32A which is possibly rather "active" since it

© American Astronomical Society • Provided by the NASA Astrophysics Data System

© American Astronomical Society • Provided by the NASA Astrophysics Data System

TABLE 2B

OBSERVED (F) REDDENING-CORRECTED (F_0) RELATIVE EMISSION LINE FLUXES FOR HERBIG-HARO OBJECTS OBSERVED WITH THE MCSP

Ion	Line (A)	H-H 3 F	H-H 3 F_0	H-H 7 F	H-H 7 F_0	H-H 11 F	H-H 11 F_0	H-H 32 F	H-H 32 F_0
[OII]	3726/29	126.4	193.8	66	81	67	81	206.4	396.0
H12	3750	5.9	9.0	-	-	-	-	1.2	2.3
H11	3770	*	*	*	*	*	*	1.1	2.2
H10	3798	*	*	*	*	*	*	(0.6)	(1.0)
H9	3835	*	*	*	*	*	*	5.1	9.3
[NeIII]	3868	*	*	(<18)	(<23)	-	-	8.9	15.5
H8	3888	*	*					7.8	13.4
CaII	3933	5.3	7.4	(37)	(43)	63	74	8.9	14.9
CaII [NeIII] H7	3968	*	*					11.4	18.5
[SII]	4069/76	16.6	21.9	(49)	(57)	87	99	47.9	73.0
Hδ	4101	23.8	30.7	(25)	(28)	-	-	16.2	24.1
[FeII]	4114	*	*	*	*	*	*	13.3	19.5
[FeII]	4230	9	11	-	-	-	-	3.6	4.9
[FeII]	4287	*	*	*	*	*	*	3.3	4.4
[FeII]	4319	*	*	*	*	*	*	1.5	1.9
Hγ	4340	*	*	68	74	50	54	29.8	38.4
[FeII] [OIII]	4359 4363	4.7	5.7	-	-	-	-	8.1	10.4
[FeII]	4414/16	3.1	3.5	20	22	-	-	7.0	8.6
[FeII]	4452/58	*	*	*	*	*	*	4.3	5.2
He I	4471	*	*	*	*	*	*	3.8	4.5
MgI]	4571	6.3	6.9	-	-	-	-	3.0	3.4
[FeIII]	4658	*	*	*	*	*	*	7.8	8.6
HeII	4686	*	*	*	*	*	*	3.8	4.1
[FeII] [FeIII]	4728 4734	7.1	7.4	-	-	-	-	3.0	3.2
[FeII]	4815	*	*	*	*	*	*	2.3	2.3
Hβ	4861	100.00	100.0	100.0	100.0	100.0	100.0	100.0	100.0
[FeII]	4889/05							5.2	5.1
[OIII]	5959	*	*	*	*	*	*	31.7	28.0
[OIII]	5007	48.2	44.4	(<17)	(<16)	(<7)	(<7)	93.8	85.2
[FeII]	5111	*	*					3.4	2.9
[FeII]	5158	*	*					15.7	12.9
[NI]	5200	17.1	14.7	164	153	178	166	16.2	12.9
[FeII]?	5220			*	*	*	*	2.2	1.7

Ion	Line (A)	H-H 3 F	H-H 3 F_0	H-H 7 F	H-H 7 F_0	H-H 11 F	H-H 11 F_0	H-H 32 F	H-H 32 F_0
[FeII]	5262	*	*					8.0	6.1
[FeII]	5273	*	*	*	*	*	*	13.0	9.9
[FeII]	5333	5.2	4.2	_	_	_	_	13.7	2.7
[FeII]	5376	9.6	7.7	-	-	-	-	<2	<1
[FeII]	5527	5.6	4.2	-	-	-	-	2.0	1.3
[OI]	5577	*	*	*	*	*	*	<2	<1.5
[NII]	5755	*	*	*	*	*	*	5.7	3.3
[OI]	6300	108.4	66.8	429	343	507	405	213.5	102.0
[OI]	6363	35.2	21.4	471	377	199	159	56.0	26.1
[NII]	6548	*	*					86.8	38.6
Hα	6563	484.6	284.5	958	754	577	454	556.9	246.9
[NII]	6583	157.3	92.1	(60)	(47)	118	92	410.9	181.3
?	6667							3.3	1.4
[SII]	6717	110.5	63.3	3114	2398	884	681	200.7	85.1
[SII]	6731	*	*	*	*	*	*	325.7	137.1
He I	7065	(4.5)	(2.4)	-	-	-	-	3.3	1.4
[AIII]	7135	-	-	-	-	-	-	7.6	2.9
[FeII]	7155	*	*	*	*	83	62	35.1	13.5
[FeII]	7172	*	*	*	*	*	*	34.1	12.9
[CaII]	7291	33.2	17.3	251	185	249	184	48.9	17.9
[OII] [CaII] [OII]	7330	40.3	20.7	*	*	58	43	118.6	42.9
[FeII]?	7380	12.8	6.5	-	-	53	39	29.0	10.6
[FeII]	7688	16.4	8.2	-	-	-	-		
H (P) 9	8598	*	*	*	*	*		42.9	14.8
[FeII]	8617								
[SIII]	9069	*	*	*	*	*		(26.1)	(9.0)
[SIII]	9532							52.6	11.7
[CI]	9824	29.7	11.1	629	397	119	75	43.1	9.5
[CI]	9848	22.8	8.5	626	392	251	159	65.4	14.5
[SII]	10316	11.0	3.9	(150)	(90)	<40	<22	51.7	10.5
[SII]	10336	*	*	*	*	*	*	79.6	16.3
[NI]	10396	-	-	-	-	-	-	35.8	7.3
[NI]	10406	-	-	-	-	-	-	21.1	4.3
He I	10830	*	*	*	*	*	*	135.5	26.0

NOTE: The same explanations as for table 2A apply.

1981ApJS...47..117B

TABLE 3

Hβ FLUX IN ABSOLUTE UNITS (ergs cm^{-2} s^{-1}) OBTAINED WITH THE MCSP

Object	F	F_0
H-H 1 (NW).....	1.08×10^{-13}	5.53×10^{-13}
H-H 1 (SE)	2.09×10^{-14}	1.15×10^{-13}
H-H 2A.....	3.66×10^{-14}	1.37×10^{-13}
H-H 2G.....	4.15×10^{-14}	2.13×10^{-13}
H-H 2H.....	9.22×10^{-14}	3.09×10^{-13}
H-H 3	1.27×10^{-14}	6.30×10^{-14}
H-H 7	1.62×10^{-15}	3.41×10^{-15}
H-H 11	4.82×10^{-15}	1.02×10^{-14}
H-H 32	2.75×10^{-14}	3.18×10^{-13}

NOTE.—F=observed Hβ flux above the Earth's atmosphere in ergs cm^{-2} s^{-1}; F_0=observed Hβ flux corrected for interstellar extinction.

TABLE 4

INTEGRATION TIMES FOR IMAGE INTENSIFIED DISSECTOR SCANNER OBSERVATIONS OF HERBIG-HARO OBJECTS

Object	Wavelength Region 3600–5400 Å	Wavelength Region 4800–7400 Å
H-H 1 (NW)	3600, 2400	3600, 2400
H-H 2G	3600	...
H-H 2H	3600	2400, 2400
H-H 3	1200	4000
H-H 3 (500″W)	300	...
H-H 3 (100″W)	300	...
H-H 3 (100″E).....	300	...
H-H 11	3600	...
H-H 24A	4800	3600, 3600
H-H 30	...	1800
H-H 40	600	900

NOTE.—The total integration time is given in seconds.

shows large radial velocities as well as a large spread in radial velocities (Herbig 1978) and also a rather high degree of ionization (see Table 2). However, in view of the short time interval between the two series of observations it is also very implausible that all differences between Dopita's (1978*b*) and our observations can be explained in this way. A complete clarification of the situation may eventually come from additional independent observations. On the other hand, we feel confident that our measurements are fairly reliable since we get very similar results from our observations with the 5.08 m telescope and MCSP II and with the Kitt peak 2.13 m telescope and IIDS.

V. INTERPRETATION OF THE LINE SPECTRA

a) N_e-T_e Diagrams

It had been well established that the excitation of the forbidden lines in H-H objects was due to impacts from thermal electrons (Böhm 1956; Osterbrock 1958; Haro and Minkowski 1960; Magnan 1965). The recent discovery of a relatively strong ultraviolet continuum in H-H 1 (Ortolani and d'Odorico 1980; Böhm, Böhm-Vitense, and Brugel 1981) necessitates a reexamination of this problem, although the conclusion remains unchanged. As evidenced by the emission line spectrum of molecular hydrogen (Elias 1980), the ultraviolet radiation apparently does not seriously affect the degree of excitation. The observed line ratios of H_2 are very different from those predicted for emission by cascade after excitation by ultraviolet photons (Black and Dalgarno 1976) and are best explained in terms of collisional excitation associated with an extremely low (15 km s^{-1}) velocity shock.

Thus, considering only collisional excitation and collisional and radiative de-excitation, the relative intensities of lines originating from different levels within a given ion will be dependent upon only the electron temperature and density. Consequently, the standard statistical equilibrium procedure described by Seaton (1954) may be applied. Application of this "standard method" follows the analysis of Böhm, Perry, and Schwartz (1973); however, the original computer code has been modified

© American Astronomical Society • Provided by the NASA Astrophysics Data System

1981ApJS...47..117B

TABLE 5A

OBSERVED (F) AND REDDENING-CORRECTED (F_0) RELATIVE EMISSION LINE FLUXES FOR HERBIG-HARO OBJECTS OBSERVED WITH THE IIDS

Ion	Line (A)	H-H1 (NW) F	H-H1 (NW) F_0	H-H 2G F	H-H 2G F_0	H-H 2H F	H-H 2H F_0	H-H 3 F	H-H 3 F_0
[OII]	3726/29	189.4	294.6	144.1	217.9	160.3	211.3	294.4	450.9
H12	3750	1.0	1.5	-	-	2.0	2.7	-	-
H11	3770	-	-	-	-	1.7	2.3	-	-
H10	3798	3.0	4.5	-	-	2.5	3.4	-	-
H9	3835	2.8	4.2	5.2	7.5	2.9	3.9	-	-
[NeIII]	3868	8.5	12.4	7.7	10.9	12.3	16.3	13.1	18.9
H8	3888	8.2	11.8	7.6	10.8	9.6	12.	12.1	17.3
CaII	3993	16.1	22.7	16.1	22.2	9.5	12.2	16.2	22.5
CaII [NeIII] H7	3968	21.5	29.9	22.7	30.8	19.9	25.2	23.8	32.7
[SII]	4068	44.8	59.6	65.7	85.9	45.5	56.0	22.9	30.2
[SII]	4076	16.7	22.2	22.9	29.9	14.0	17.2		
Hδ	4101	16.4	21.5	17.7	22.8	17.6	21.4	18.6	24.1
[FeII]	4114	2.5	3.2	2.3	2.9	2.4	2.8	-	-
[FeII]	4177	(1.8)	(2.3)	1.7	2.2	1.1	1.3	-	-
[FeII]	4244	6.8	8.4	6.6	8.0	6.6	7.7	-	-
[FeII]	4276	2.3	2.8	5.4	6.4	2.6	3.0	-	-
[FeII]	4287	6.7	8.1	12.3	14.7	6.5	7.5	4.8	5.8
[FeII]	4319	2.3	2.7						
Hγ	4340	37.5	44.6	39.9	46.9	44.6	36.3	42.9	
[FeII] [OIII]	4359	10.7	12.6	14.3	16.7	11.8	13.3	10.6	12.5
[FeII]	4414/16	10.9	12.5	12.1	13.8	8.0	8.9	5.0	5.7
[FeII]	4452/58	4.6	5.2	7.1	8.0	4.4	4.8		
He I	4471	2.7	3.1	4.1	4.7	3.5	3.8	3.9	4.4
MgI]	4571	6.1	6.7	9.5	10.4	3.9	4.2	4.7	5.2
?	4580	(0.9)	(0.9)	3.0	3.3	1.2	1.3		
[FeIII]	4658	4.8	5.1	6.7	7.1	7.7	8.1	3.6	3.9
HeII	4686	1.4	1.5	1.8	1.9	1.8	1.9	-	-
[FeIII]	4702	(0.9)	(0.9)	3.0	3.1	2.1	2.2	-	-
[FeII] [FeIII]	4728 4734	1.0	1.0	3.0	3.2	3.0	3.1	-	-
?	4755	1.1	1.1	-	-	1.4	1.4	-	-
?	4776	1.2	1.2	-	-	-	-	-	-
[FeII]	4815	5.1	5.1	5.3	5.4	3.0	3.0	-	-
Hβ	4861	100.0	100.0	100.0	100.0	100.0	100.0	100.0	100.0
[FeII]	4889	4.4	4.4	(5.9)	(5.9)	4.8	4.8	-	-
[FeII]	4905	2.0	2.0	2.6	2.5	1.7	1.7	-	-
[OIII]	4959	15.5	14.9	13.6	13.2	28.0	27.2	14.2	13.7
[OIII]	5007	47.1	42.7	46.2	42.2	88.9	82.8	43.3	39.4
[FeII]	5111	2.9	2.6	2.7	2.4	1.7	1.6		
[FeII]	5128	23.9	20.9	26.7	23.5	16.6	15.1	10.8	9.5
[NI]	5200	22.8	19.5	21.0	18.2	10.2	9.1	22.9	19.7
[FeII]?	5220	1.4	1.2	-	-	1.2	1.1	-	-
[FeII]	5262	9.3	7.7	11.1	9.3	6.3	5.5	-	-
[FeII] [FeIII]	5262/73 5270	14.2	11.8	20.7	17.3	12.7	11.1	8.8	7.3
[FeII]	5333	4.1	3.3	4.9	4.0	3.6	3.1	-	-
[FeII]	5376	2.3	1.8	2.2	1.7	2.2	1.9	-	-
?	5414	1.8	1.4			2.0	1.7	-	-
[FeII]	5527	4.5	3.4			4.3	3.5	-	-
[OI]	5577	3.7	2.7			3.8	3.1	-	-
[NII]	5755	5.8	4.0			7.0	5.4	-	-
He I	5876	6.6	4.4			8.8	6.6	-	-
[OI]	6300	181.4	109.9			162.4	112.7	163.0	100.5
[OI]	6363	57.6	34.3			52.5	36.0	47.0	28.5
Hα	6563	410.3	236.3			423.7	283.4	382.1	224.3
[NII]	6583	171.6	98.5			199.8	133.4	140.5	82.4
?	6667	1.8	1.0			1.5	1.0	-	-
He I	6678	1.9	1.1			3.1	2.0	-	-
[SII]	6717	74.4	41.6			57.8	37.8	329.6	187.9
[SII]	6731	126.1	70.1			102.6	66.7		
He I	7065	2.1	1.1			2.5	1.6	-	-
[AIII]	7135	1.1	0.6			2.8	1.7	-	-
[FeII]	7155	20.8	10.9			14.5	9.1	-	-
[FeII]	7172	4.6	2.4			4.5	2.8	-	-
CaII	7291	23.6	12.1			13.0	7.9	47.1	24.5

NOTE: the standardnormalization F(Hβ) = 100. has been used.

© American Astronomical Society • Provided by the NASA Astrophysics Data System

1981ApJS...47..117B

TABLE 5B

OBSERVED (F) AND REDDENING-CORRECTED (F) RELATIVE EMISSION LINE FLUXES FOR HERBIG-HARO OBJECTS OBSERVED WITH THE IIDS

Ion	Line (A)	H-H 11 F	H-H 11 F_o	H-H 24A F	H-H 24A F_o	H-H 30 F	H-H 30 F_o	H-H 40 F	H-H 40 F_o
[OII]	3726/29	111	134	71	139			138	267
[NeIII]	3868	-	-	-	-	-	-	6	10
CaII	3933	(76)	(92)	14	24	-	-	8	14
[SII]	4069	(77)	(88)	26	40	-	-	} 26	41
[SII]	4076	(31)	(36)	13	20	-	-		
Hδ	4101	-	-	15	23	-	-	11	17
Hγ	4340	-	-	33	43	-	-	30	39
[FeII]	4414/16	-	-	-	-	-	-	4	5
MgI]	4571	-	-	5	6	-	-	·7	8
Hβ	4861	100.0	100.0	100.0	100.0	(100)	(100)	100.0	100.0
[OIII]	4959	-	-	14	13	-	-	26	24
[OIII]	5007	-	-	26	22	-	-	69	60
[FeII]	5158	(51)	(48)	19	15	-	-	29	16
[NI]	5200	206	192	36	28	(30)	-	30	24
[FeII]	5262/73	-	-	16	12	-	-	16	12
[OI]	5577	-	-	<6	<4	-	-	<5	<3
(NII]	5755	-	-	<6	<4	-	-	<5	<4
[OI]	6300			221	103	526		161	76
[OI]	6363			72	33	165		78	36
[NII]	6548			64	28				
Hα	6563			528	228	813		512	214
[NII]	6583			168	72	132		208	91
[SII]	6717			179	74	358		} 389	163
[SII]	6731			246	101	443			
[FeII]	7155			14	15	-			
[FeII]	7172			6	2	-			
CaII	7291			(12)	(4)			(39)	(14)

NOTE: The usual normalization F(Hβ)= 100. has been used.

TABLE 6

DETERMINATIONS OF INTERSTELLAR REDDENING

Object	$E(B-V)$	Error	$A(\mathrm{H}\beta)$
H-H 1 (NW) ...	0.47	(0.05)	1.81
H-H 2A	0.37	(0.08)	1.43
H-H 2G	0.44	(0.05)	1.69
H-H 2H	0.34	(0.05)	1.31
H-H 3	0.45	(0.08)	1.73
H-H 7	(0.21)	...	(0.81)
H-H 11	0.21	(0.15)	0.81
H-H 32	0.69	(0.05)	2.66
H-H 24A	0.71	(0.20)	2.73
H-H 40	0.70	(0.20)	2.70

NOTE.—The $E(B-V)$ value for H-H 7 has been adopted from the H-H 11 calculation. $E(B-V)$ for H-H 11 is based on somewhat uncertain [S II] 10316 data (see Böhm, Brugel, and Mannery 1980).

and [O II] (Pradhan 1976) have been incorporated. The sources of atomic data for C I, N I, N II, O I, O III, and Ne III can be found in Böhm, Perry, and Schwartz (1973). The collisional de-excitation parameters for Ca II are taken from Shine (1974).

Theoretical predictions of desired flux ratios were calculated, and the locus of points corresponding to each observed flux ratio was plotted in the N_e-T_e plane. In an idealized situation, all of these curves would pass through a single point and thus uniquely determine the electron temperature and density. In practice the intersection is not a point but rather a general "crossing region." Several factors influence the size of this crossing region, including inhomogenities in N_e and T_e throughout the nebula (as they do occur in the recombination regions of shock waves), uncertainties in the atomic parameters, and errors in the observed line strengths.

Each data set (MCSP and IIDS) has been separately utilized in the construction of N_e-T_e diagrams for 10 of the observed condensations (Figs. 1–11). Solid lines have been used to depict those line ratios which originate from the same multiplet or from different multiplets of the same ion. These curves will be considered the "primary indicators" of the physical parameters N_e and T_e. Long dashed lines represent an abundance independent ratio of lines of [N I], [O I], [N II], and [O II]; dotted lines represent those line ratios which are considered to be "secondary indicators". These "secondary indicators" are dependent upon abundance and ionization assumptions discussed in Böhm, Perry, and Schwartz (1973). The [O II] line ratio 3726+3729 Å/7318+7330 Å is also plotted as a dotted curve since

© American Astronomical Society • Provided by the NASA Astrophysics Data System

1981ApJS...47..117B

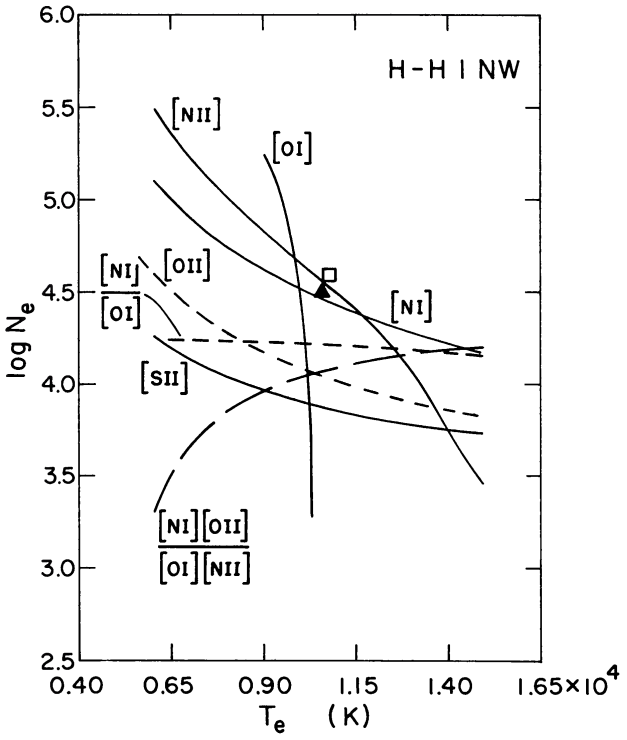

FIG. 1

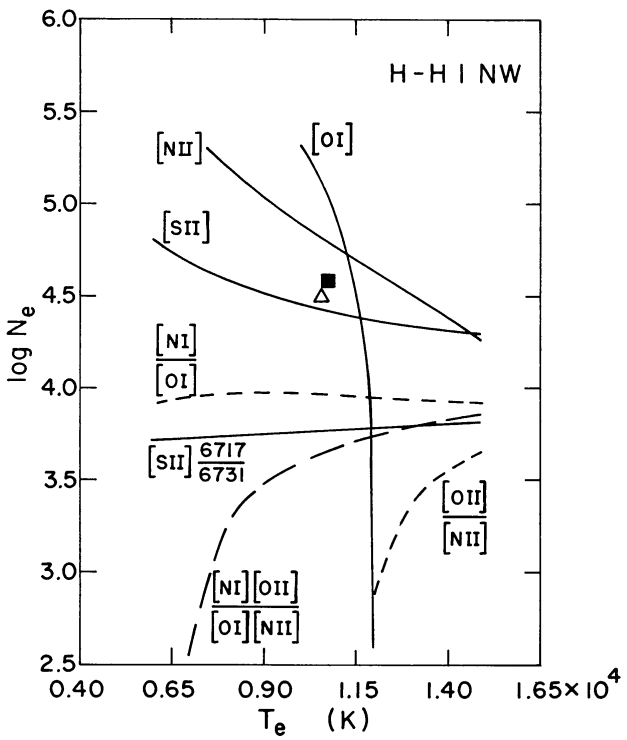

FIG. 2

FIG. 1.—N_e-T_e diagram for forbidden line ratios observed in H-H 1 (NW) with the MCSP. The solid curve marked [O I] refers to the flux ratio λ5577/(λ6300+6363), [S II] to λ6717/(λ4068+4076), [N I] to λ5200/(λ10396+10406), and [N II] to λ5755/(λ6548+6583). These are "primary indicators" as defined in the text. The long-dashed curve marked [N I] [O II]/[O I] [N II] refers to the ratio (λ5200)(λ3726+3729)/(λ6300+6363)(λ6548+6583). The "secondary indicators" (see text) are distinguished by short-dashed curves. The curve marked [N I]/[O I] refers to [λ5200/(λ6300+6363)], and [O II] refers to [(λ3726+3729)/(λ7318+7330)]. The value for N_e-T_e derived from these data is marked with a filled triangle; the IIDS result for this object (Fig. 2) is designated by an open square.

FIG. 2.—N_e-T_e diagram for forbidden line ratios observed in H-H 1 (NW) with the IIDS. The meaning of the curve markings is the same as in Fig. 1. The value for N_e-T_e derived from these data is marked with a filled square; the MCSP result for this object (Fig. 1) is designated by an open triangle.

the "observed" intensity ratio depends upon a theoretical deconvolution of the observed [Ca II], [O II] complex centered at 7330 Å. The theoretical [Ca II] line ratio 7323/7291 Å, calculated by the previously described statistical equilibrium procedure, appears to be a constant (0.67) for T_e between 5000 and 20,000 K and log N_e between 3.0 and 6.0.[3] Since 7291 Å of [Ca II] is observed, it is possible to determine the implied 7323 Å [Ca II] flux contribution to the [Ca II]+[O II] blend and thus obtain the 7318+7330 Å line strength of [O II]. Obviously, one must be cautious in interpreting values of N_e and T_e based solely on this line ratio.

The existence of temperature and density inhomogenities within H-H objects readily explains some systematic displacements of individual curves in the N_e-T_e plane. Theoretical computations illustrate that the [S II] lines λλ6717/6731, the [N I] line λ5200, and the [O II] line λ3726+3729 have reasonably large emissivities at low density. On the other hand, emissivities of the [S II] lines λλ4067+4076, the [O I] lines λλ6300+6363, the [N I] lines λλ10396+10406, and all three visual lines of [N II] decrease rapidly with decreasing density. Thus, for example, the [N II] λ5755/(6548+6583) ratio provides primarily information about the high density regions, while the [S II] λ6717/6731 ratio includes some information about the low density regions. The [O II] lines λλ3726+3729 possess the largest low to high density emissivity ratio; therefore, an appreciable fraction of the total observed flux in these lines will probably originate from low density regions. These relationships between emissivity and density have significant bearing on any interpretation of the N_e-T_e diagrams.

The line strength ratios of [N II] λ5755/(6548+6583), [N I] λ5200/(10396+10406), and [O I] λ5577/(6300+6363) provide the best estimates of N_e and T_e in the high density regions. The [O I] ratio is particularly important since it is primarily temperature dependent. Unfortunately, the 5577 Å line is extremely weak for most objects, in addition to being contaminated by the [O I] night sky line; thus, for some objects, it has been neces-

[3]Preliminary reductions of high dispersion spectroscopic observations of H-H 1 (Brugel and Wallerstein 1981) confirm this theoretical predication.

© American Astronomical Society • Provided by the NASA Astrophysics Data System

1981ApJS...47..117B

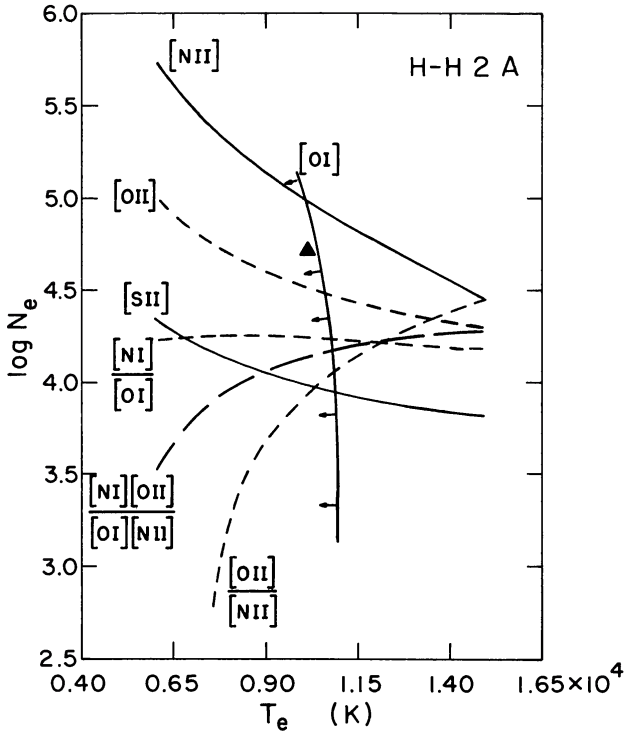

FIG. 3.—N_e-T_e diagram for forbidden line ratios observed in H-H 2A with the MCSP. The meaning of the curve markings is the same as in Fig. 1. The value for N_e-T_e derived from these data is marked with a filled triangle.

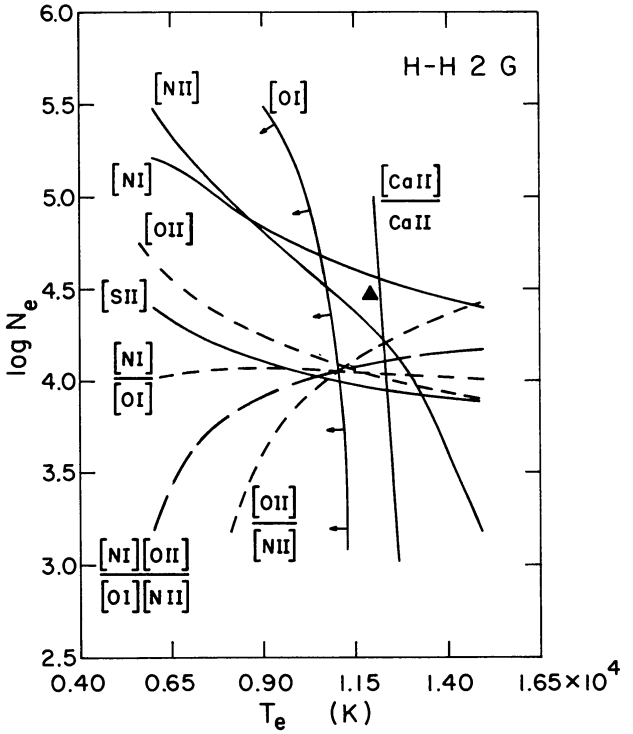

FIG. 4.—N_e-T_e diagram for forbidden line ratios observed in H-H 2G with the MCSP. The meaning of the curve markings is the same as in Fig. 1. The value for N_e-T_e derived from these data is marked with a filled triangle.

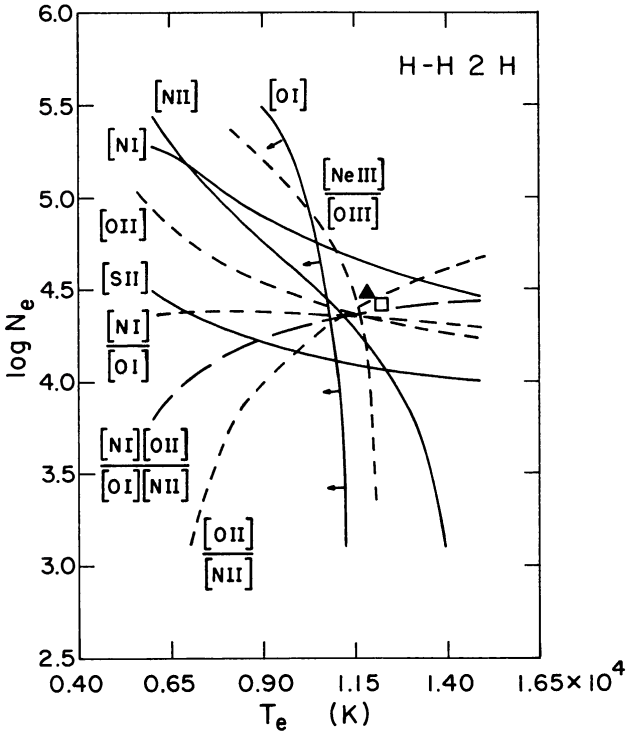

FIG. 5.—N_e-T_e diagram for forbidden line ratios observed in H-H 2H with the MCSP. The meaning of the curve markings is the same as in Fig. 1. The value for N_e-T_e derived from these data is marked with a filled triangle; the IIDS result for this object (Fig. 6) is designated by an open square.

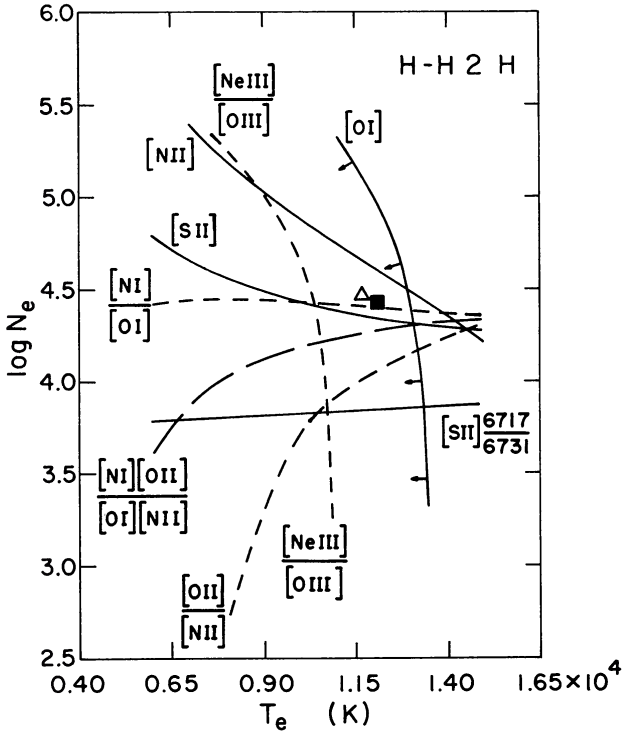

FIG. 6.—N_e-T_e diagram for forbidden line ratios observed in H-H 2H with the IIDS. The meaning of the curve markings is the same as in Fig. 1. The value for N_e-T_e derived from these data is marked with a filled square; the MCSP result for this object (Fig. 5) is designated by an open triangle.

© American Astronomical Society • Provided by the NASA Astrophysics Data System

1981ApJS...47..117B

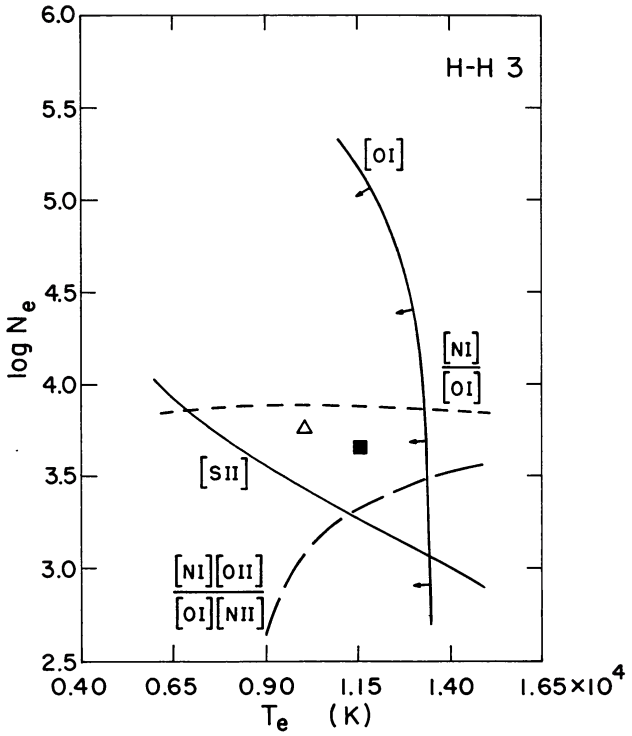

FIG. 7.—N_e-T_e diagram for forbidden line ratios observed in H-H3 with the MCSP. The meaning of the curve markings is the same as in Fig. 1. The value for N_e-T_e derived from these data is marked with a filled triangle; the IIDS result for this object (Fig. 8) is designated by an open square.

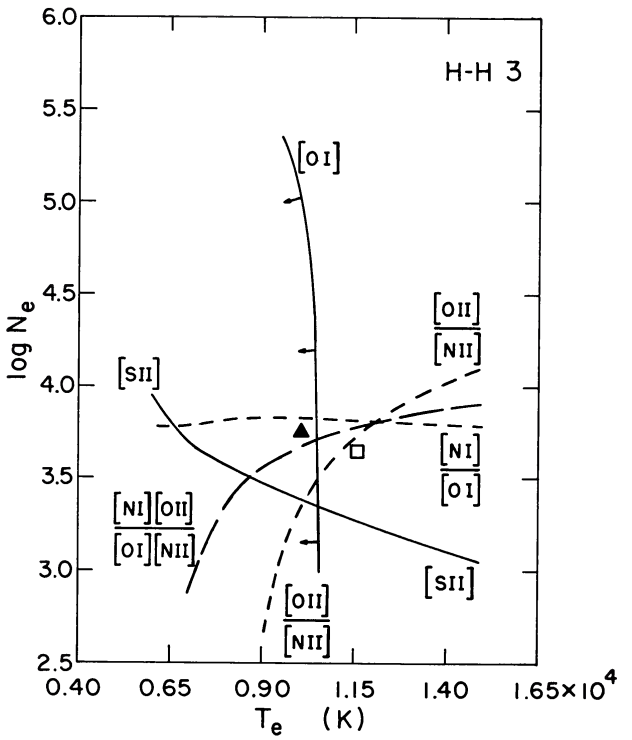

FIG. 8.—N_e-T_e diagram for forbidden line ratios observed for H-H 3 with the IIDS. The meaning of the curve markings is the same as in Fig. 1. The value for N_e-T_e derived from these data is marked with a filled square; the MCSP result for this object (Fig. 7) is designated by an open triangle.

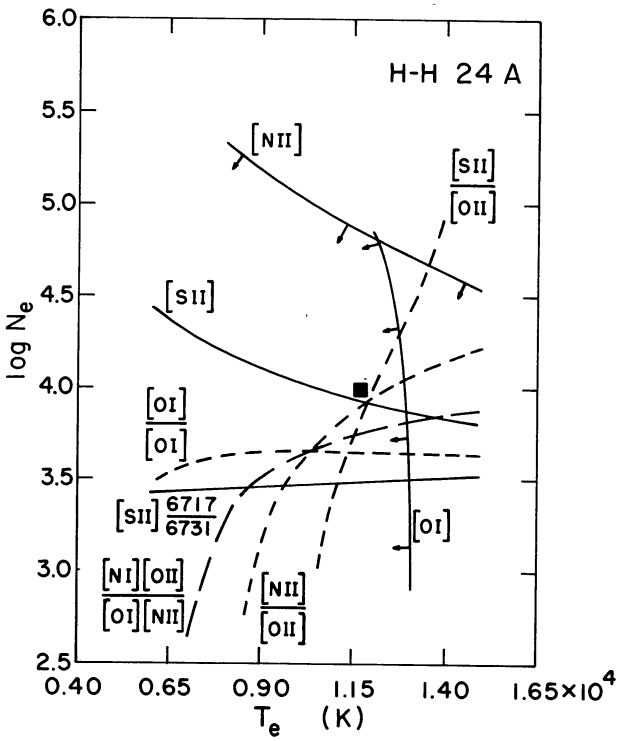

FIG. 9.—N_e-T_e diagram for forbidden line ratios observed in H-H 24A with the IIDS. The meaning of the curve markings is the same as in Fig. 1. The value for N_e-T_e derived from these data is marked with a filled square.

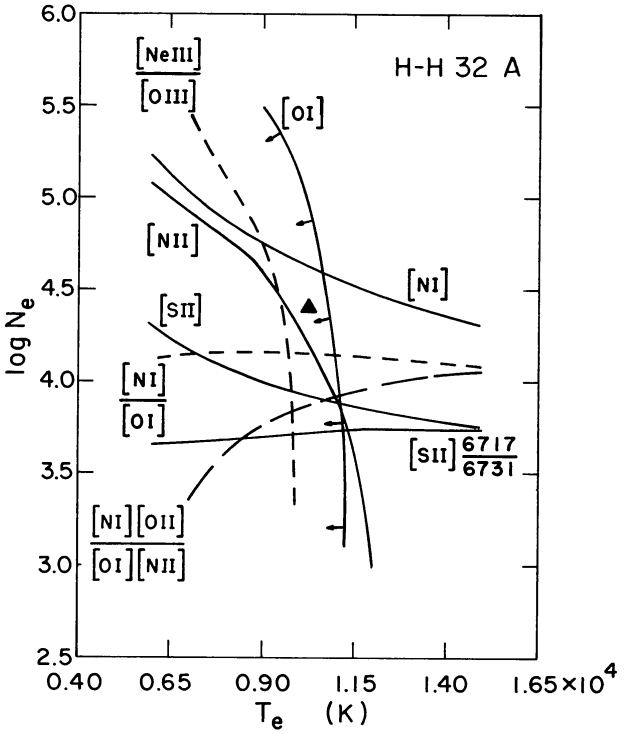

FIG. 10.—N_e-T_e diagram for forbidden line ratios observed in H-H 32 with the MCSP. The meaning of the curve markings is the same as in Fig. 1. The value for N_e-T_e derived from these data is marked with a filled triangle.

© American Astronomical Society • Provided by the NASA Astrophysics Data System

1981ApJS...47..117B

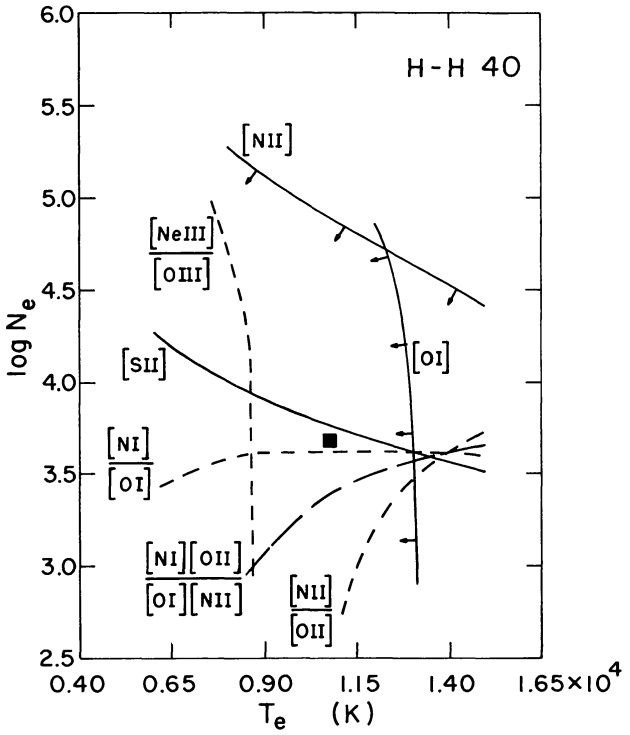

FIG. 11.—N_e-T_e diagram for forbidden line ratios observed in H-H 40 with the IIDS. The meaning of the curve markings is the same as in Fig. 1. The value for N_e-T_e derived from these data is marked with a filled square.

sary to determine an upper limit for the strength of this line. In principle, the sky subtraction procedure should alleviate the night sky contamination problem; however, for a very weak 5577 Å line the difference between the object plus sky and the sky alone is very small and correspondingly uncertain. Similarly, upper limits for 5755 Å of [N II] had to be derived for H-H 24A and H-H 40.

Values of T_e and N_e representative of the high density regions are indicated on each N_e-T_e diagram. Squares mark the values implied by the IIDS data alone; triangles indicate the MCSP II results. To avoid confusion, the N_e-T_e diagrams of each object will be discussed separately. The uncertainty in the electron temperature determined in this manner is typically 500 K but may be as high as 1000 K for the fainter objects in which there are fewer observed line ratios. Similarly, the uncertainty in $\log N_e$ is $\sim$0.2, but may be as large as 0.4.

Böhm, Siegmund, and Schwartz (1976) derived values of $T_e = 10{,}200$ K and $N_e = 3.0 \times 10^4$ cm^{-3} for brightest region (NW) of H-H 1; the high density crossing regions of Figures 1 and 2, with $T_e = 10{,}600$ K and $N_e = 3.4 \times 10^4$ cm^{-3}, are in essential agreement with this earlier result. Thus, the present analysis indicates that no significant changes in the physical conditions within this object have occurred during the period 1973 Jan to 1978 Sep. Nonetheless, a continuation of the trend of increasing temperature and density already noted (Böhm, Siegmund, and Schwartz 1976) may possibly be inferred from these results, although the uncertainty in N_e and T_e exceeds the implied increases. Being more conservative, these observations do at least confirm the density increase from $N_e = 2.0 \times 10^4$ cm^3 in 1969 (Böhm, Perry, and Schwartz 1973) to $N_e = 3.2 \times 10^4$ cm^{-3} in 1973 (Böhm, Siegmund, and Schwartz 1976).

The MCSP and IIDS results for the high density crossing region of H-H 1 show reasonable agreement. However, the "low density" line ratios (e.g., [N I]/[O I], [N II]/[O II], and [N I] [O II]/[O I] [N II]) show considerable systematic displacements. The functions $N_e(T_e)$ derived from the IIDS data (for these line ratios) indicate lower densities than the MCSP observations. This trend is a direct consequence of larger relative line strengths observed with the IIDS for the lines of [N I] (5200 Å) and [O II] (3726+3729 Å). This apparent observational discrepancy is consistent with a model which characterizes Herbig-Haro objects in terms of two regions consisting of low and high density (see § V*d*). Since the low density component makes up the largest fractional volume of the object, observations taken through a larger aperture should show increased relative line strengths for those lines formed predominately in the low density regions. Obviously this situation arises only for more extended objects, in which their angular diameters exceed the aperture size. The IIDS observations, taken with an aperture 44% larger in area then the MCSPs, produced [N I] and [O II] line strengths which are 40% and 30% larger, respectively. It is thus strongly suggested that these differences are due solely to density inhomogenities within H-H 1.

Further information pertaining to the low density region is provided by the [S II] line ratio λλ6717/6731. An electron density of $\sim 5.6 \times 10^3$ cm^{-3} is implied by this curve (see Fig. 2). This value of N_e should be interpreted as an upper limit for the low density region, since the observed line fluxes probably include substantial emissions from the higher density regions.

The crossing region for H-H 2A (Fig. 3) is not very well determined. The [O I] line ratio (λ5577/6400+6363) provides an upper limit for the temperature of $T_e < 10{,}300$ K. The accepted electron density, $N_e = 5.4 \times 10^4$ cm^{-3}, is bracketted by the line ratios of [N II] and [O II]. The lower densities implied by the [N I]/[O I] and [N I] [O II]/[O I] [N II] curves are probably indicative of density inhomogenities within the condensation.

For condensation G of H-H 2, an electron temperature of 12,000 K is indicated by the Ca II/[Ca II] (λ3933/7291) line ratio (Fig. 4). A density of $N_e = 3.5 \times 10^4$ cm^{-3} is well established by the [N I] and [N II] curves. These values are consistent with the earlier results of $N_e = 5 \times 10^4$ cm^{-3} and $T_e < 13{,}000$ K obtained in 1973 (Böhm, Siegmund, and Schwartz 1976).

© American Astronomical Society • Provided by the NASA Astrophysics Data System

1981ApJS...47..117B

The N_e-T_e diagrams for H-H 2H (Figs. 5 and 6) indicate $T_e = 11{,}800$ K and $N_e = 3.0 \times 10^4$ cm^{-3}. By comparison, observations taken in 1973 by Böhm, Siegmund, and Schwartz (1976) indicate $T_e = 11{,}400$ K and $N_e = 2.5 \times 10^4$ cm^{-3}, while data acquired in 1975 (Böhm and Brugel 1979) revealed $T_e = 12{,}000$ K and $N_e = 2.0 \times 10^4$ cm^{-3}. Lacking a consistent trend in these results, it is difficult to determine if any real variations in N_e and T_e have occurred over this fairly short time span. However, both sets of data taken in 1978 confirm the more than 50% increase in the [S II] λ6717+6731 line strength which occurred during the interval 1973 Jan–1975 Feb (Böhm and Brugel 1979).

The "low density" curves (e.g., [N I]/[O I] and [N I] [O II]/[O I] [N II]) for both the MCSP and the IIDS observations are unusually consistent with the high density crossing region. This consistency may imply that the high density regions of H-H 2H produce a greater percentage of the observed line fluxes than seen in other condensations. Nonetheless, the [S II] line ratio (λ6717/6731) does indicate the existence of a low density component with an upper limit of $N_e < 7 \times 10^3$ cm^{-3}.

The [O I] ratio (λ5577/6300+6363) provides a reasonable estimate of the electron temperature ($T_e = 10{,}500$ K) for H-H 3 (Figs. 7 and 8). The electron density is considerably more uncertain, although a value of $N_e = 6 \times 10^3$ cm^{-3} seems appropriate for both the IIDS and MCSP data.

The N_e-T_e diagrams for H-H 7 and H-H 11 based upon this MCSP data can be found in Böhm, Brugel, and Mannery (1980). The derived physical parameters are $N_e = 2.5 \times 10^3$ cm^{-3}, $T_e = 7500$ K for H-H 7, and $N_e = 2.5 \times 10^3$ cm^{-3} and $T_e = 9300$ K for H-H II.

The N_e-T_e diagram for H-H 24A (Fig. 9) presents a fairly compact high density crossing region delineated by the curves of [S II] (λ6717/4068+4076), [S II]/[O II] and [N II]/[O II]. The upper limit designated by the [O I] line ratio is also reasonably consistent with these curves. However, the upper limit curve for [N II] is disparate with all other line ratios and thus ignored. The parameters $T_e = 11{,}700$ K and $N_e = 1.0 \times 10^4$ cm^{-3} are therefore unfortunately based upon only two "primary indicators" ([S II] and [O I]). The low density line ratio of [S II] (λ6717/6731) indicates a density of $N_e = 2.8 \times 10^3$ cm^{-3} and implies significant density inhomogenities in this object.

For H-H 32 (Fig. 10) values of $T_e = 10{,}100$ K and $N_e = 2.7 \times 10^4$ cm^{-3} are well established and based upon the line ratios of [O I], [N I] [N II], and [Ne III]/[O III]. In addition, the ratio λ6717/6731 of [S II] indicates a low density of $N_e < 5.6 \times 10^3$ cm^{-3}, while the curves of [N I]/[O I] and [N I] [O II]/[O I] [N II] also imply the existence of a significant low density region.

It is difficult to define a unique crossing region for H-H 40 (Fig. 11). This is partly so because the [O I] and [N II] curves are only identified as upper limits. Nonetheless, the electron temperature is probably near 10,900 K based on a mean between the [O I] and [N_e III]/[O III] curves. An electron density $N_e = 4.7 \times 10^3$ cm^{-3} is indicated by the line ratios of [S II] and [N I]/[O I].

To summarize, the electron temperatures determined from all of these N_e-T_e diagrams possess a relatively narrow dispersion (2000 K) centered around 10,500 K. Apparently the electron temperatures of the emitting regions do not vary greatly from object to object. The electron density, however, varies by more then a factor of 20 in the extreme. Furthermore, the existence of H-H objects with high (H-H 1), medium (H-H 24A), and low (H-H 7) density may imply that this class of nebulae possess a complete density continuum over an interval from N_e equal to ~1000 to several tens of thousands cm^{-3}. The actual density range might be even greater since the derived lowest value of N_e may not be a true lower limit. Any object with a substantially lower N_e may be unobservable with present detectors.

b) Determinations of N_e via the Hβ Flux

The observed absolute Hβ flux can be used to directly calculate the electron density if it is assumed that the number density of H II ions is equal to the electron number density. This assumption is justified for H-H objects considering the negligible ionization of helium indicated by its relatively weak emission lines. For Menzel's case (*b*) and an electron temperature of 10,000 K, the emissivity (emission per unit volume) of Hβ is (cf. Aller and Liller 1968)

$$E(\mathrm{H}\beta) = 1.241 \times 10^{-25} N(\mathrm{H\ II}) N_e. \qquad (2)$$

Thus, the observed flux (corrected for reddening) received at the top of the Earth's atmosphere for a spherical gas cloud of radius r (a.u.) and distance d (pc) is

$$F(\mathrm{H}\beta) = 1.454 \times 10^{-23} (r^3/d^2) N(\mathrm{H\ II})^2, \qquad (3)$$

where it is assumed that $N(\mathrm{H\ II}) = N_e$. The input parameters and resulting mean number density of H II ions in the emitting region are listed in Table 7. Note that the absolute Hβ fluxes for H-H 24A and H-H 40 are taken from Dopita (1978*b*). All of the H-H objects observed herein, with the exception of H-H 32, are apparently associated with the Orion OB association, thus placing them at a distance of 500 pc. The linear radii listed in Table 7 for the extended nebulae H-H 1 (NW), H-H 3, H-H 7, and H-H 24A correspond to the angular entrance aperture through which the observations were taken. For the condensations of H-H 2 the linear radii correspond to angular radii estimated from the photograph published by Herbig (1969). The angular radii for H-H 11 and H-H 40 were estimated from the photographs in Herbig's catalog (1974). Using an assumed

© American Astronomical Society • Provided by the NASA Astrophysics Data System

1981ApJS...47..117B

TABLE 7

PHYSICAL PARAMETERS OF OBSERVED HERBIG-HARO OBJECTS

Object	d(pc)	r(au)	dia	F(Hβ)	L(Hβ)	L(line)	N(HII)	X(HII)	M	T_e (K)	log N_e
H-H 1	500	1250	5."0	3.76	16.54	291	2210	0.49	16.9	10,600	4.53
H-H 2A	500	500	2."0	5.83	4.10	66	4340	0.80	2.1	10,250	4.74
H-H 2G	500	500	2."0	9.06	6.37	99	5410	0.59	2.7	12,000	4.54
H-H 2H	500	500	2."0	13.1	9.21	141	6520	0.69	3.2	11,800	4.48
H-H 3	500	900	3."6	0.87	1.98	21	1200	0.69	3.5	10,500	3.78
H-H 7	500	1750	7."0	0.012	0.103	5.4	105	0.10	2.2	7,500	3.40
H-H 11	500	375	1."5	0.77	0.305	9.0	1820	0.07	0.4	9,300	3.38
H-H 24A	500	1525	6."1	1.56*	10.2*	118*	1050*	0.45	14.6*	11,700	4.00
H-H 32	500	1250	5."0	2.17	9.51	260	1670	0.62	12.8	10,100	4.44
H-H 40	500	1000	4."0	0.96*	2.70*	34*	1245*	0.27	4.9*	10,900	3.68

NOTE: Explanation of symbols
F(Hβ) = surface H Beta brightness in 10^{-3} ergs/cm2/s
L(Hβ) = total H Beta flux in 10^{30} ergs/s
L(line) = total energy emitted by all observed lines (Table 2) in 10^{-3} ergs/s
N(HII) : derived from emission measure of Hβ
x(HII) = fractional ionization of hydrogen estimated from OI ionization
M = mass of ionized hydrogen only, in earth masses
T_e, log N_e : derived from forbidden lines

TABLE 8

FILLING FACTORS FOR THE PRINCIPLE EMISSION LINES SEEN IN HERBIG-HARO OBJECTS

		FILLING FACTOR times FRACTIONAL IONIZATION (IN UNITS OF 10^{-3})									
Ion	Line	H-H1(NW)	H-H2A	H-H2G	H-H2H	H-H3	H-H7	H-H11	H-H24A	H-H32A	H-H40
OI	6300+6363	0.50	1.11	3.03	5.40	3.60	0.55	49.6	0.79	0.51	2.86
OII	3726+3729	1.16	4.41	4.22	7.52	4.70	0.04	3.26	0.55	2.28	3.46
OIII	4959+5007	0.039	0.26	0.18	0.71	0.52	<.003	0.16	0.046	0.10	0.30
SII	4069+4076	0.86	1.88	6.06	10.49	5.67	0.37	71.56	2.01	1.32	7.09
SII	6717	3.28	9.68	19.87	23.84	11.08	3.82	151.3	2.76	3.50	6.57
SII	6731	2.30	-	-	17.7	-	-	-	1.94	2.39	6.57
SII	10318	0.80	1.97	4.81	9.39	5.48	-	86.15	-	1.03	-
SIII	9532	0.096	0.26	-	1.23	-	-	-	-	0.14	-
NeIII	3869	0.12	0.78	1.36	3.28	5.48	<.15	<6.95	-	0.46	1.87
CI	9824+9848	0.04	0.30	0.37	0.58	0.37	0.13	5.82	-	0.09	-
NI	5200	1.05	3.34	8.93	8.14	4.05	0.56	63.9	1.51	1.01	3.55
NI	10396/406	0.88	1.98	9.56	11.87	-	-	-	-	1.63	-
NII	5755	0.68	3.21	2.56	7.63	-	-	-	<1.33	0.77	<6.61
NII	6548+6583	0.65	2.22	3.31	9.33	4.31	0.03	8.21	0.59	0.92	2.75
CaII	3933	0.36	0.43	1.78	3.13	1.97	0.25	42.95	0.86	0.37	2.21
CaII	7291	0.23	0.21	1.70	2.10	1.98	0.24	37.27	-	0.18	1.01
MgI	4571	0.014	0.016	0.07	0.56	0.22	-	-	0.028	0.014	0.17
HI	4861	4.29	6.32	24.4	46.63	41.0	1.73	578.3	11.1	3.69	67.5

NOTE: OIII filling factors for H-H 3, H-H 7 and H-H 11 are based on λ5007 only. N II filling factor determinations for all objects except H-H 1 and H-H 32A have not used λ6583.

distance of 500 pc, the entrance aperture also defines the linear radius for H-H 32.

The electron density calculated in this manner is $\langle N_e^2 \rangle^{1/2}$ and is generally 5–15 times smaller than that derived from the emission line ratios. It has been known for some time that the emitting volume of H-H objects is only partially filled with emitting material (Böhm, Siegmund, and Schwartz 1976). The object H-H 11 is exceptional in that it appears to be almost totally filled with radiating matter, as is indicated by the fact that the electron densities computed from the Hβ emission and from the forbidden line strengths are approximately equal.

The total mass of protons in each condensation has also been calculated and tabulated (Table 7). In each case, the total mass of emitting material is only on the order of a few Earth masses.

c) *Calculation of Filling Factors*

Since the MCSP data is calibrated in absolute units, it is possible to determine the filling factor or fractional volume which a given ion must fill (at the temperature and density determined by the $N_e - T_e$ diagram) to produce the observed flux of any emission line of that ion. Theoretical line emissivities (energy emitted per s

© American Astronomical Society • Provided by the NASA Astrophysics Data System

1981ApJS...47..117B

per ion) are calculated by the statistical equilibrium computer program described in § V*a*, for the ions/atoms O I, O II, O III, N I, N II, S II, S III, Ca II, Ne III and C I. In the case of 4571 Å of Mg I, the emissivity is calculated based upon a simple two-level atom (Osterbrock and Dufour 1973).

Essentially the quantity filling factor (ϵ) times fractional ionization x is determined by equating the observed absolute line flux with a predicted flux based upon the theoretical line emissivity. A detailed description of this procedure is given by Böhm, Siegmund, and Schwartz (1976).

The quantity ϵx has been calculated for the majority of emission lines and is presented in Table 8. The filling factor for a given element can be ascertained by summing ϵx over all ionization stages of that element.

The average filling factor for oxygen is less than 0.02, where H-H 7 possesses the smallest (0.59×10^{-3}) and H-H 11 the largest (53.0×10^{-3}) value. These results correspond to linear dimension ratios of roughly 0.08 to 0.38. The emission lines for all these objects are obviously formed in exceedingly small volumes compared to the total extent of the object (or even the individual condensation).

d) *Empirical Models of the Line Formation Regions in Herbig-Haro Objects*

The N_e-T_e diagrams discussed in § IV*a* provide rather convincing evidence that the regions of line formation possess a high degree of inhomogeneity. Following the example of Böhm, Siegmund, and Schwartz (1976), this inhomogeneous characteristic is used as the basis for the construction of two-component models for the following objects: H-H 1 (NW), H-H 2A, H-H 2G, H-H 2H, and H-H 32. These empirical models simplify the inhomogeneous nature of these objects by assuming that the observed emission lines are formed in only two separate regions of high and low density. The models are specified by the density and filling factor in each of these domains.

The derived high and low density components are not in static pressure equilibrium, which is understandable considering the nature of these objects. Herbig-Haro nebulae have been shown to be fairly rapidly varying objects (Herbig 1969), and the line forming regions are probably associated with highly supersonic flows (Schwartz 1975).

In the calculation of these models, it is assumed that the degree of ionization of hydrogen is equal to the fractional ionization of O I (Böhm, Siegmund, and Schwartz 1976). This value of N(H II)/N(H) and the electron temperature determined from the N_e-T_e diagram are also presumed to be appropriate for both components. The value of N_e in the low-density region is initially set equal to 1×10^3 cm^{-3}. This simplification is justified by the following argument. The [S II] λλ6717/6731 line ratios for H-H 1 (NW), H-H 2H, and H-H 32 imply an upper limit for N_e (in the low density region) on the order of 5×10^3 cm^{-3} (§ IV*c*); thus, a density of 1×10^3 cm^{-3} is reasonably consistent. Additionally, in the case of H-H 1 (NW), where the [O II] λ3726/3729 ratio has been resolved (Böhm, Perry, and Schwartz 1973), a density of 2×10^3 cm^{-3} is implied. Regarding the high density region, the value of N_e inferred from the N_e-T_e diagram is used as an initial indication of the electron density for this component.

Final values for the electron density–filling factor pairs are determined by requiring that these parameters define a model which reproduces the observed [S II] and [N II] line ratios within the observational errors, and that the sum of the fractional ionizations of O I, O II, and O III equal unity. The solutions are obtained by a trial and error procedure described by Böhm, Siegmund, and Schwartz (1976). The resulting model parameters are given in Table 9.

These models are obviously not unique, as indicated by the large number of free parameters and limited number of constraints. Nonetheless, the existence of at least two distinct density regions are strongly suggested by the N_e-T_e diagrams discussed in § IV*a*.

The data for H-H 3, H-H 7, H-H 11, H-H 24A, and H-H 40 are insufficient for the determination of two-component models. Thus, for these objects, exceedingly simplistic homogeneous models have been constructed. The model parameters are also listed in Table 9.

Relative ion abundances are also ascertained from these empirical models. This information is obtained in the following manner. The magnitude of the filling factors is scaled such that the sum of the fractional ionizations (abundances) of the three oxygen ions is equal to one. This fixes the ion abundances onto the same scale, assuming the Population I (Allen 1973) abundance ratio of the element relative to oxygen. Consequently, if the elemental abundances are standard Population I and the model parameters are correct, then the relative ion abundances will give that fraction of an element present in the observed ionization stages. The computed ion abundances are presented in Table 10. The percentages of the flux in each line which is formed in the high-density region are also listed.

The details of any single model should not be taken as the final quantitative description for the structure of any particular H-H object; rather it is the sum total of all these model results which establishes a reasonably convincing general description of Herbig-Haro condensations. This simple structural picture emerges from the following features inherent in all five of the two-component models. As previously noted for H-H 1 (NW) and H-H 2H alone (Böhm, Siegmund, and Schwartz 1976), the high density region, which produces the majority of the emission line flux, always fills an exceedingly small percentage of the total volume, typi-

© American Astronomical Society • Provided by the NASA Astrophysics Data System

1981ApJS...47..117B

TABLE 9A

BASIC PARAMETERS FOR THE EMPIRICAL TWO-COMPONENT MODELS

	H-H 1 (NW)		H-H 2A		H-H 2G		H-H 2H		H-H 32	
REGION	(1)	(2)	(1)	(2)	(1)	(2)	(1)	(2)	(1)	(2)
T_e	10600	10600	10250	10250	12000	12000	11800	11800	10100	10100
N_e	1×10^3	3.2×10^4	1×10^3	4.0×10^4	1×10^3	$2\times3\times10^4$	1×10^3	6.3×10^4	1×10^3	2.5×10^4
ff.....	0.38	6.6×10^{-4}	2.8	3.4×10^{-3}	1.73	7.3×10^{-3}	3.06	1.9×10^{-3}	0.43	1.4×10^{-3}
H II/H	0.49	0.49	0.80	0.80	0.59	0.59	0.69	0.69	0.62	0.62
F.....	0.08	0.14	0.15	0.29	0.06	0.13	0.07	0.17	0.15	0.32

NOTE.—ff = filling factor, F = ratio of theoretical to observed Hβ flux.

TABLE 9B

BASIC PARAMETERS OF EMPIRICAL HOMOGENOUS MODELS

Region	H-H 3 (1)	H-H 7 (1)	H-H 11 (1)	H-H 24A (1)	H-H 40 (1)
T_e	10500	7500	9300	11700	10900
N_e	6.0×10^3	2.5×10^3	2.4×10^3	1.0×10^4	4.8×10^3
ff	8.8×10^{-3}	5.9×10^{-4}	5.3×10^{-2}	1.4×10^{-3}	9.3×10^{-3}
H II/H ...	0.69	0.10	0.07	0.45	0.27
F	0.22	0.33	0.09	0.13	0.14

NOTE.—ff = filling factor, F = ratio of theoretical to observed Hβ flux.

TABLE 10A

IONIC ABUNDANCES (A in %) AND PERCENTAGES OF LINE FLUXES FORMED IN HIGH-DENSITY REGIONS (f)

		H-H1(NW)		H-H-2A		H-H2G		H-H2H		H-H32	
ION	LINE	A	f	A	f	A	f	A	f	A	f
O I	5577		64		-		67		68		68
O I	6300+6363	42	49			61	65	47	72	29	66
O II	3726+3729	55	28	50	26	35	37	48	24	65	35
O III	4959+5007	4	62	10	67	4	66	6	69	6	66
N I	5200	36	21	27	19	52	27	30	15	22	27
N I	10396/406		80		83		80		85		84
N II	5755		69		72		70		77		71
N II	6548+6583	55	55	75	55	55	60	81	57	47	61
S II	4069+4076		79		82		79		85		82
S II	6717	128	25	97	24	163	32	109	21	94	32
S II	6731		45		-		52		40		52
S III	9532	10	64	9	65		-	2	98	8	67
Ca II	3933	31	66	13	67	36	66	23	71	16	68
Ca II	7291		64		69		66		70		69
Ne III	3869	13	61	30	65	28	66	29	71	26	67
C I	9824+9848	2	30	4	29	3	37	3	24	3	37
Mg I	4571	.6	84	.6	65	2	69	1	69	.6	67

cally less than a few tenths of a percent. Conversely, the low density region virtually fills the entire object, at a density comparable to the surrounding molecular cloud medium.

Furthermore, the low density region, by virtue of its large filling factor, is also the place of origin for a major portion of the [O II] (λ3726/3729), [N I] (λ5200), and [S II] (λ6717/6731) emission line fluxes, as indicated in Table 10. This conclusion essentially agrees with the previously discussed interpretation of the N_e-T_e diagrams (§ IVa).

Derived elemental abundances (A) (based upon the two-component models) for H-H 1 (NW), H-H 2A, H-H 2G, H-H 2H, and H-H 32, expressed relative to "cosmic" (Allen 1973) Population I abundance (A_c), are displayed in Figure 12. The results are relatively consistent from object to object, as well as being compatible with the assumed "cosmic" abundances. For several elements

© American Astronomical Society • Provided by the NASA Astrophysics Data System

1981ApJS...47..117B

TABLE 10B

IONIC ABUNDANCE (A in %)

ION	LINE	H-H 3 A	H-H 7 A	H-H 11 A	H-H 24A A	H-H 40 A
O I	5577					
O I	6300+6363	41	93	94	57	43
O II	3726+3729	53	7	6	40	52
O III	4959+5007	6	.5	.3	3	5
N I	5200	46	94	121	109	54
N I	10396/406					
N II	5755					
N II	6548+6583	49	5	15	43	42
S II	4069+4076		62	135		
S II	6717	95	644	285	161	103
S II	6731					
Ca II	3933	22	42	76	62	24
Ca II	7291					
Ne III	3869	62	<25	<13	-	28
C I	9824+9848	4	22	11	-	-
Mg I	4571	3	-	-	2	3

NOTE: For H-H 3, H-H 7 and H-H 11, the O III information is derived from λ5007 only. The second line of the N II information is based on 6583 only for H-H 2A, H-H 2G, H-H 2H, H-H 3, H-H 7, H-H 11, H-H 24A, H-H 40.

only a single ionic species is observed; in these cases the ratio A/A_c is necessarily less than one. In particular, the Mg I abundances are exceedingly small (~1%–2% of the "cosmic" Mg abundance), which is not surprising considering the ionization potential is only 7.65 eV. Presumably magnesium exists primarily in higher ionization states, particularly Mg II. There is some limited empirical evidence to validate this hypothesis. For H-H 1 (and probably H-H 2H), the blended ultraviolet Mg II lines λλ2796/2803 are moderately strong (Böhm, Böhm-Vitense, and Brugel 1981), indicating considerable Mg II abundance. The mean Ca II abundance (for all five objects) is 24%(±10%) of the "cosmic" Ca abundance;[4] this value may be considered high in light of its ionization energy (11.87 eV).

The low C I abundance (mean value of ~3%[±0.6%] of the "cosmic" C abundance) is a bit perplexing. The ionization potential for C I is only 0.6 eV less than the Ca II energy. Therefore, it is reasonable to expect the C I abundance to be similiar to the Ca II abundance, not a factor of 8 less as observed. No convincing explanation for this paradox is presently available, although the ultraviolet spectrum may provide a clue. The presence of strong emission lines of C II (1335 Å), [C III] (1909 Å), and even C IV (1548+1550 Å) (Ortolani and d'Odorico 1980; Böhm, Böhm-Vitense, and Brugel 1981) may indicate a much higher degree of ionization for carbon than

[4]The stated dispersion is not indicative of the uncertainty in the abundance determinations but rather refers to the spread in the computed values from object to object. Actual variations in the ionic abundances are expected between objects due to differences in the degree of excitation.

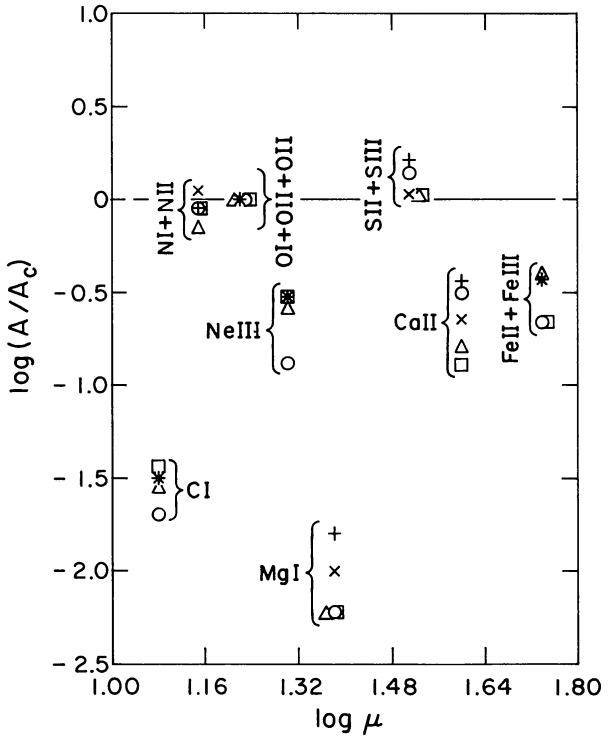

FIG. 12.—The logarithm of the ratio of the observed element abundances to the "cosmic" abundances (Allen 1973) in H-H 1 (NW) (*circles*), H-H 2A (*squares*), H-H 2G (*plus marks*), H-H 2H (*crosses*), and H-H 32 (*triangles*). The elements are designated by the logarithm of the atomic weight. For H-H 2G the sulfur abundance refers to S II only.

© American Astronomical Society • Provided by the NASA Astrophysics Data System

1981ApJS...47..117B

is suggested from the Ca II argument. Furthermore, it is interesting to note that the objects with the lowest overall excitation (H-H 7 and H-H 11) also have much greater ionic abundances for C I, 22% and 11% of the "cosmic" C abundance, respectively.

The total nitrogen (N I+N II) and sulfur (S II+S III) ionic abundances (mean abundances equaling 96% [±17%] and 124%[±25%] of "cosmic," respectively) clearly demonstrate that these five objects possess normal ("cosmic") elemental abundances. The fact that no metal deficiencies are evident, particularly for Ca, is not a totally expected result. One might have anticipated, in regions of star formation, to observe gas-phase deficiencies for the refractory elements (i.e., Ca and Fe) (Spitzer and Jenkins 1975; Salpeter 1977) due to the creation of dust grains.

The homogeneous models for H-H 3, H-H 7, H-H 11, H-H 24A, and H-H 40 have also been employed in the derivation of chemical compositions for these objects. The results are displayed in Figure 13. These calculations are very preliminary and susceptible to much greater uncertainty then the two-component model results. Specifically, the assumption of homogeneity, which is only marginally tenable, and the weakness of some observed emission lines are the major contributing factors to this uncertainty. Nonetheless, the abundances determined are also consistent with the conclusions derived from the more accurate two-component models. It is worthwhile to reemphasize that in no case is there any evidence for metal depletion due to dust formation in an Herbig-Haro object.

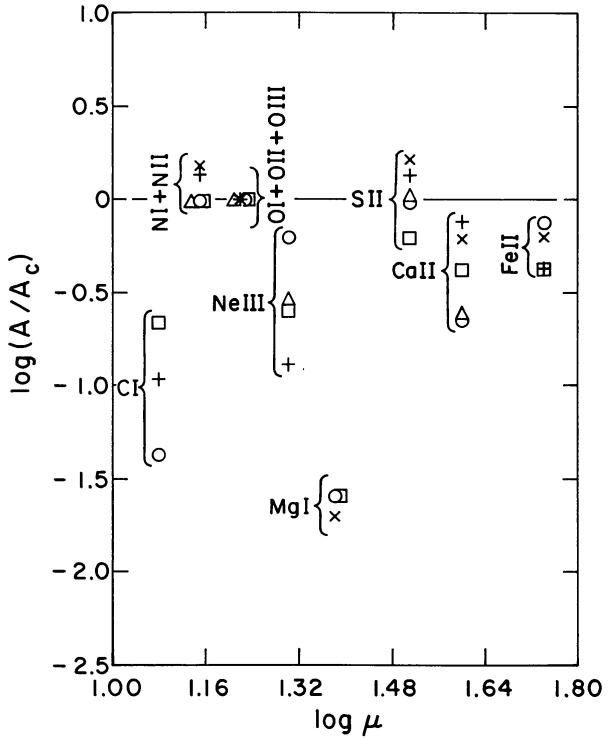

FIG. 13.—The logarithm of the ratio of the observed element abundances to the "cosmic" abundances (Allen 1973) in H-H 3 (*circles*), H-H 7 (*squares*), H-H 11 (*plus marks*), H-H 24A (*crosses*), and H-H 40 (*triangles*). The elements are designated by the logarithm of the atomic weight. For H-H 3 the iron abundance refers to Fe II+Fe III.

e) Derivation of the Iron Abundance via the [Fe II] *and* [Fe III] *Line Spectra*

A program for calculating the standard statistical equilibrium condition for Fe III and Fe II has been described by Böhm and Brugel (1979) and is used herein for the derivation of ionic abundances for iron.

Emission lines of [Fe III] are detected in a limited number of objects: H-H 3 and H-H 32. Unfortunately only a single line, 4658 Å, is observed at a reasonable strength (typically 5%–8% of Hβ) and unblended with other emission lines. The fainter [Fe III] lines at 4734, 4814.8/4815.1, and 5720 Å may have also been observed. However, they are very faint and blended with [Fe II] lines. The line at 5011 Å also seems to be faintly present in the wing of the strong line [O III] λ5007, although blended beyond recovery. The only other unblended [Fe III] line observed is 4702 Å; however, it is extremely weak and therefore highly uncertain. Consequently, the Fe III abundance determinations depend almost entirely on the strongest [Fe III] line λ4658. Keep in mind that this line is well identified and free of blends and even a crude determination of the Fe abundance is of considerable importance since in some interstellar clouds Fe is sometimes depleted by as much as a factor of 100 to several hundred (Spitzer and Jenkins 1975; Salpeter 1977).

In order to make these results directly comparable to the previously discussed abundance determinations, the quantity (εx) is evaluated for [Fe III]. The results have been listed in Table 11. Typically the Fe III abundance is ~10% of the "cosmic" Fe abundance. This conclusion does not look unreasonable since the [Fe II] lines are on the average considerably stronger than the [Fe III] lines.

A crude estimate of (εx) for Fe II has also been made although these results must be given much lower weight than those for Fe III. The main difficulty is that quantum mechanical collisions strengths for Fe II are not available. This difficulty has been "overcome" in a very naive way. The collisional excitation cross sections for the Fe II transitions have been calculated using the classical theory as essentially given by Woolley and Stibbs (1953) and described by Böhm and Brugel (1979).

The Fe II abundances are also based upon calculations of (εx); determinations for the individual lines of [Fe II] are listed in Table 12. Lines for which the flux is five or smaller (on a scale of Hβ=100) and for which the spectrophotometry is correspondingly uncertain are shown in parenthesis. Values for the computed Fe II abundance based upon a mean of the individual calcula-

© American Astronomical Society • Provided by the NASA Astrophysics Data System

1981ApJS...47..117B

TABLE 11

FILLING FACTORS AND ABUNDANCE DETERMINATIONS FOR [Fe III]

Object	$F_0(\lambda 4658)$	$F_0(\lambda 4702)$	Filling Factor (Fe III/Fe)	$A(\%)$
H-H 1 (NW) ...	4.15	...	0.110	6.5
H-H 1 (NW) ...	...	0.90	0.080	4.7
H-H 2A	8.80	...	0.658	11.4
H-H 2G	6.25	...	0.907	12.2
H-H 2H	7.30	...	2.445	17.9
H-H 3	3.90	...	1.380	15.6
H-H 32	8.60	...	0.295	10.2

NOTE.—F_0 is the mean of the MCSP and the IIDS line fluxes. Filling factors are given in units of 10^{-3}. The ionic abundance A (in percent of the "cosmic" abundance) is derived using the total filling factor for oxygen.

TABLE 12

FILLING FACTORS AND ABUNDANCE DETERMINATIONS FOR THE EMISSION LINES OF [Fe II]

	FILLING FACTOR times FRACTIONAL IONIZATION FeII/Fe (10^{-3})								
Line	H-H1 (NW)	H-H2A	H-H2G	H-H2H	H-H3	H-H11	H-H24A	H-H32	H-H40
4114	(0.63)		(2.61)	(5.77)					
4244	0.33		1.48	3.47					
4276	(0.22)		2.36	(2.68)					
4287	0.11							(0.80)	
4319	(0.33)							(0.32)	
4815	0.38		1.97	2.64				(0.23)	
4889	(0.18)		1.35	2.57				0.29	
4905	0.34		(2.11)	(3.47)				(1.19)	
5111	(0.25)		(1.18)	(1.88)				(0.37)	
5158	0.28	(0.14)	1.60	2.42	2.30	27.9	0.44	0.23	2.34
5220	0.11			(1.21)				(0.21)	
5262	0.25	0.60	1.52	2.15	4.24		0.88	0.26	(4.12)
5273	(0.27)	1.07	2.41	(3.28)	10.2		1.91	0.79	
5333	(0.13)	(0.21)	(0.81)	(1.48)	(2.80)			(0.14)	
5376	(0.09)	(0.16)	(0.44)	1.14	6.42			(0.66)	
5527	(0.14)	(0.36)	(0.73)	(1.77)	(3.19)			(0.70)	
7155	0.25	0.48	1.56	2.39		17.2	0.28	0.15	
7172	0.30	0.75	4.44	2.98				0.47	
MEAN	0.26	0.56	1.89	2.54	5.23	22.6	0.88	0.37	2.93
Error	45%	55%	51%	39%	58%	34%	84%	78%	35%
A(%)	15	10	25	19	59	43	63	30	44

NOTE: This is a list of filling factors times fractional ionization (εx) in units of 10^{-3}. A is the average abundance of FeII in percent.

tions of (εx) are also tabulated. Lines in parentheses are given half-weight in determining the mean value. The sum of the Fe II+Fe III ionic abundances lies between 22% (for H-H 1 [NW]) and 40% (for H-H 32) of the "cosmic" Fe abundance (see Fig. 12). Since no information is available for neutral Fe, the total iron abundance may be somewhat higher.

These results are clearly compatible with a normal Population I abundance of Fe and show no indication of any strong depletion due to dust formation.

The lack of observational data prevents a derivation of the Fe III abundance of several objects (H-H 11, H-H 24A, and H-H 40). Nonetheless, preliminary indications of the elemental iron abundance based only on Fe II should not be totally ignored. These results (shown in Fig. 13), although highly uncertain on observational and theoretical grounds, are again consistent with a normal Population I abundance.

The fact that Fe and Ca do not appear to be depleted in H-H 24A is significant. The highly polarized continuum observed in this object (Schmidt and Miller 1979) has been interpreted "as reflected emission from a nearby star" due to scattering by dust. However, the existence of enhanced dust concentrations within H-H 24A is not manifested by gas-phase deficiences in the refractory elements. A possible explanation is that the emission lines and the continuum originate in two separate and distinct regions. In this context, photo-

© American Astronomical Society • Provided by the NASA Astrophysics Data System

1981ApJS...47..117B

graphs taken at continuum wavelengths (e.g. 5400–6200 Å) and in individual emission lines (e.g., Hα, Hβ, [N II]) may resolve this apparent inconsistency.

To reiterate the abundance analysis, Herbig-Haro objects possess normal Population I "cosmic" abundances. This conclusion is not unexpected in light of their ages (Strom, Grasdalen, and Strom 1974). Additionally, although H-H objects occur only in regions of recent star formation in which a considerable amount of dust is present, there is no indication of either Ca or Fe depletion due to dust formation "inside" Herbig-Haro objects.

One possible explanation for the latter unexpected result has already been expressed by Böhm and Brugel (1979). Sputtering of dust grains may occur in the shock waves, whose cooling regions lead to the formation of the emission line spectra of H-H objects. If this should be correct it would probably imply that at some earlier time the shock velocity has been higher than it is now (shock velocities on the order of 50–100 km s^{-1} are inferred by the emission line spectra; see Raymond 1976, 1979; Dopita 1978*a*, *b*) because higher shock speeds (>200 km s^{-1}) are required to destroy the relevant grains (cf. Salpeter 1977). This result is highly interesting since (if correct) it reveals something about the development of the shock wave. On the other hand, recently acquired ultraviolet spectral data (Ortolani and D'Odorico 1980; Böhm, Böhm-Vitense, and Brugel 1981) may imply that higher velocity shocks also exist in H-H objects.

f) *Helium Recombination Spectra*

The ionic abundance of singly ionized helium has been determined according to the method of Robbins, Daltabuit, and Cox (1979) and Drake and Robbins (1972), as described by Böhm, Siegmund, and Schwartz (1976). These determinations are based upon the He I lines λλ4471 (4^3D–2^3P), 5876 (3^3D–2^3P), and 10830 (2^3P–2^3S). The theoretical intensities of these lines relative to the intensity of H are expressed by the following relationships:

$$\frac{I(4471)}{I(4681)} = \frac{4861}{4471}\frac{\beta(4^3D)+q(2^3S-4^3D)N(2^3S)}{\alpha_{\rm eff}(\mathrm{H}\beta)} \times \frac{N(\mathrm{He\ II})}{N(\mathrm{H\ II})}, \quad (4)$$

$$\frac{I(5876)}{I(4861)} = \frac{4861}{5876}\frac{\beta(3^3D)+q(2^3S-3^3D)N(2^3S)}{\alpha_{\rm eff}(\mathrm{H}\beta)} \times \frac{N(\mathrm{He\ II})}{N(\mathrm{H\ II})}, \quad (5)$$

$$\frac{I(10830)}{I(4861)} = \frac{4861}{10830}\times\frac{\beta(2^3P)+q(2^3P)+q(2^3S-2^3P)N(2^3S)}{\alpha_{\rm eff}(\mathrm{H}\beta)}\frac{N(\mathrm{He\ II})}{N(\mathrm{H\ II})}, \quad (6)$$

where $N(2^3S)$ is the ratio of the population of the 2^3S state to the number of helium ions, β is the effective recombination rate including cascades, q is the thermally averaged collisional excitation rate, and $\alpha_{\rm eff}(\mathrm{H}\beta)$ is the rate of hydrogen recombinations which result in Hβ photons. Equations (5) and (6) are from Böhm, Siegmund, and Schwartz (1976). Substituting values for q from Drake and Robbins (1972) and using Brocklehurst's (1972) determinations for β, it follows (from eqs. [4–6]) that

$$\frac{N(\mathrm{He\ II})}{N(\mathrm{H\ II})} = \frac{68.9}{33.7+10^6N(2^3S)}\frac{I(4471)}{I(4861)}, \quad (7)$$

$$\frac{N(\mathrm{He\ II})}{N(\mathrm{H\ II})} = \frac{36.1}{32.7+10^6N(2^3S)}\frac{I(5876)}{I(4861)}, \quad (8)$$

$$\frac{N(\mathrm{He\ II})}{N(\mathrm{H\ II})} = \frac{0.228}{0.203+10^6N(2^3S)}\frac{I(10830)}{I(4861)}. \quad (9)$$

The quantity $q(2^3S$–$3^3D)$ has been reduced by a factor of 3 as suggested by Brocklehurst (1972). The population of the 2^3S level can be determined by two methods. The condition of detailed balance can be solved in a purely theoretical manner (see eq. [7] of Böhm, Siegmund, and Schwartz 1976), or theory (statistical equilibrium calculation for 2^3S, 2^3P, and 3^3D) and observation can be combined to express the 2^3S population in terms of the intensity ratio $I(10830)/I(5876)$ (eq. [10] of Böhm, Siegmund, and Schwartz 1976).

A determination of $N(2^3S)$ based upon the observed triplet strengths has been performed for H-H 1 (NW) and H-H 2H since the He I line λ5876 has been detected in both these objects. Results using the 2^3S population balance equation have also been obtained for H-H 1 (NW) and H-H 2H, as well as H-H 2A, H-H 2G, H-H 3, and H-H 32. These conclusions are given in Table 13. The derived He II ionic abundances appear consistent with the "cosmic" abundance of helium if the degree of ionization of helium is much less than that of hydrogen. This assumption is verified later in this section.

It is somewhat misleading to make no mention of the radiative transfer problem associated with the metastable 2^3S state of He I, although this complication has insignificant effects in H-H objects. A post facto calcu-

© American Astronomical Society • Provided by the NASA Astrophysics Data System

1981ApJS...47..117B

TABLE 13

INFORMATION ON HELIUM EMISSION

	H-H1 (NW)		H-H2H		H-H2A	H-H2G	H-H3	H-H32
METHOD	(1)	(2)	(1)	(2)	(2)	(2)	(2)	(2)
$N(2^3S)\times10^6$ ...	4.08	2.26	3.53	3.84	3.26	3.08	1.49	1.89
He II/H II.....	0.040	0.053	0.057	0.055	0.047	0.031	0.086	0.028
τ (λ10839).....	7.5	6.9	11.0	12.4	6.1	3.0	1.6	4.5
τ (λ3889).....	0.32	0.30	0.46	0.52	0.26	0.13	0.07	0.19
He III/H II	0.001		0.001		...	0.002	...	0.003
He II/He I.....	0.10		0.12		0.12	...	...	0.12
He/H.....	0.22		(0.35)		(0.34)	...	...	0.15

NOTE.—The first line identifies the method used to determine the level population: (1) triplet line fluxes; (2) theoretical population balance. The (He II/He I) ionization ratio has been estimated from the S III/ (S II+S III) ionization ratio.

lation of the optical depth at 10830 and 3889 Å (using the absorption coefficients given by Drake and Robbins 1972) forms the basis for neglecting the line transfer problem. The optical depth at 10830 Å, for all objects (see Table 13), is sufficiently small that depopulation of the 2^3S state via the (2^3P–1^1S) transition is unimportant (cf. Drake and Robbins 1972). In addition, the very low optical thickness at 3889 Å (see Table 13) indicates that the observed lines are negligibly enhanced by absorption of photons originating from the n^3P-2^3S series (Robbins 1968).

It is possible to obtain a crude estimate of the fractional ionization of He II based upon the observed S II ionization. Since the ionization potentials of He I and S II are very similar (24.6 and 23.4 eV, respectively), it is not unreasonable to assume that the degrees of ionization are approximately equal. Thus,

$$\frac{N(\text{He II})}{N(\text{He I})+N(\text{He II})} \approx \frac{N(\text{S III})}{N(\text{S I})+N(\text{S II})+N(\text{S III})}. \quad (10)$$

If the sulfur lines are formed in the same region (as indicated for 4068+4076 and 9532 Å by the two-component models), then the fractional ionization of S III can be expressed in terms of the observed flux (F) and the theoretical emissivity (j) (see O I ionization in Böhm, Siegmund, and Schwartz 1976). Thus,

$$\frac{N(\text{S III})}{N(\text{S I})+N(\text{S II})+N(\text{S III})} = \frac{(F/j)_{\text{S III}}}{(F/j)_{\text{S I}}+(F/j)_{\text{S II}}+(F/j)_{\text{S III}}}; \quad (11)$$

it can be argued, based upon its low ionization potential, that the S I abundance is negligible and can be ignored. This is confirmed by the fact that even in the brightest objects the [S I] line at 7726 Å is not detected. Therefore, by using equations (10) and (11), the fractional ionization of He II can be ascertained. These results expressed as N(He II)/N(He I) are listed in Table 13.

A first-order approximation to the He/H ratio can be obtained by incorporating the results for N(He II)/N(He I), N(He II)/N(H II), and N(H II)/N(H) into a single expression. Specifically,

$$\frac{\text{He}}{\text{H}} \approx \frac{\text{He I}+\text{He II}}{\text{H}} = \left[\frac{N(\text{He I})}{N(\text{He II})}+1\right]\frac{N(\text{He II})}{N(\text{H III})}\frac{N(\text{H II})}{N(\text{H})}. \quad (12)$$

The marginal detections of very weak 4686 Å (He II) in H-H 1 (NW), H-H 2G, H-H 2H, and H-H 32 indicate that the He III abundance is very small, and its inclusion does not significantly alter these results. Assuming that the 4686 Å line is produced by recombination of He III, the ratio N(He III)/N(H II) can be determined from the following expression:

$$\frac{N(\text{He III})}{N(\text{H III})} = \frac{4686}{4861}\frac{\alpha_{\text{eff}}(4686)}{\alpha_{\text{eff}}(\text{H}\beta)}\frac{I(4686)}{I(4861)}, \quad (13)$$

where $\alpha_{\text{eff}}(4686)$ is the effective recombination coefficient for the He II line. This ratio is typically a few tenths of a percent and confirms the insignificance of the He III abundance relative to He I and He II. The results are included in Table 13. Derived values for He/H of 0.22 and 0.15 in the brighter objects (H-H 1 NW and H-H 32, respectively) are in fair agreement with the "cosmic" He/H ratio of 0.08. Considering the uncertainties in the extremely weak helium line strengths and the crude assumptions employed, errors of a factor of ~2 are not unexpected. For the fainter objects H-H 2A and H-H 2H the results (He/H=0.34 and 0.35) are even more uncertain, and it is impossible to formulate a meaningful conclusion.

© American Astronomical Society • Provided by the NASA Astrophysics Data System

1981ApJS...47..117B

VI. CONCLUSIONS

Analysis of the emission line spectra leads to the following conclusions:

1) The physical conditions within H-H 1 (NW) have shown no significant detectable changes during the period 1973 Jan to 1978 Sep.

2) Values for the electron density and electron temperature have been determined for 10 separate H-H condensations. From these results, it is apparent that the electron temperatures do not vary greatly from object to object, while the densities range from a few thousand to several tens of thousands cm^{-3}.

3) The observed masses of emitting material within these H-H objects lie in the range 0.4–16.9 Earth masses, with an average value of 6.3 Earth masses. This places H-H objects among the lowest mass objects detected outside of our solar system and presents an interesting association of planetary-mass objects with objects in the earliest stages of stellar evolution.

4) Significant inhomogenities in the line forming regions of these H-H objects are indicated by the derived N_e-T_e diagrams. This inhomogeneous characteristic leads to the construction of empirical two-component models for five H-H objects (H-H 1 [NW], H-H 2A, H-H 2G, H-H 2H, and H-H 32). These models describe an underlying low density region ($N_e = 1. \times 10^3$ cm^{-3}) virtually full of emitting material and a high density component which fills only a few tenths of a percent of the total volume. Although this high density region has an extremely small filling factor, the majority of the emission flux originates from this component. Similar homogeneous models have been computed for H-H 3, H-H 7, H-H 11, H-H 24A, and H-H 40.

5) These models have been employed in the determination of the ionic abundances of O I, O II, O III, N I, N II, S II, S III, Ca II, Ne III, C I, and Mg I. In all cases, these abundances are consistent with "cosmic" Population I elemental abundances.

6) Approximate iron abundances, based upon the [Fe II] and [Fe III] lines, have also been determined. These results are again consistent with a Population I abundance for all of the studied H-H objects.

7) The determined Ca and Fe abundances indicate no depletion of refractory elements due to enhanced dust formation inside a Herbig-Haro object.

8) The ratio He/H ascertained for H-H 1 (NW) and H-H 32 is in reasonable agreement with the "cosmic" helium abundance.

We are very grateful to Dr. J. B. Oke and Ms. Barbara Zimmerman for introducing us to the MCSP II system and for patient help and advice.

We also wish to thank the staff at Kitt Peak National Observatory, especially William Halbedel for his assistance at the telescope and Jeanette Barnes for her demonstration of the IIDS reduction program.

This research has been supported by NSF grants AST-7820542 and AST-7820542 A01.

REFERENCES

Allen, C. W. 1973, *Astrophysical Quantities* (3rd ed.; London: Athlone), p. 30.
Aller, L. H., and Liller, W. 1968, in *Nebulae and Interstellar Matter*, ed. B. M. Middlehurst and L. H. Liller (Chicago: University of Chicago Press), p. 483.
Black, J. H., and Dalgarno, A. 1976, *Ap. J.*, **203**, 132.
Böhm, K. H. 1956, *Ap. J.*, **123**, 379.
Böhm, K. H., Böhm-Vitense, E., and Brugel, E. W. 1981, *Ap. J. (Letters)*, **245**, L113.
Böhm, K. H., and Brugel, E. W. 1979, *Astr. Ap.*, **74**, 297.
Böhm, K. H., Brugel, E. W., and Mannery, E. 1980, *Ap. J. (Letters)*, **235**, L37.
Böhm, K. H., Perry, J. F., and Schwartz, R. D. 1973, *Ap. J.*, **179**, 149.
Böhm, K. H., Siegmund, W. A., and Schwartz, R. D. 1976, *Ap. J.*, **203**, 399.
Brocklehurst, M. 1972, *M.N.R.A.S.*, **157**, 211.
Brugel, E. W., Böhm, K. H., and Mannery, E. 1981, *Ap. J.*, **243**, 874.
Brugel, E. W., and Wallerstein, G. 1981, in preparation.
Dopita, M. A. 1978*a*, *Astr. Ap.*, **63**, 237.
_____. 1978*b*, *Ap. J. Suppl.*, **37**, 117.
Drake, G. W. F., and Robbins, R. R. 1972, *Ap. J.*, **171**, 55.
Elias, J. H. 1980, *Ap. J.*, **241**, 728.
Haro, G., and Minkowski, R. 1960, *A.J.*, **65**, 490.
Herbig, G. H. 1969, in *Non-Periodic Phenomena in Variable Stars*, ed. L. Detre (Dordrecht: Reidel), p. 75.
Herbig, G. H. 1974, *Lick Obs. Bull.*, No. 658.
_____. 1978, private communication.
Magnan, C. 1965, *C. R. Acad. Sci., Paris*, **261**, 3294.
Miller, J. S. 1968, *Ap. J. (Letters)*, **154**, L57.
Oke, J. B. 1969, *Pub. A. S. P.*, **81**, 11.
Ortolani, S., and d'Odorico, S. 1980, *Astr. Ap.*, **83**, L8.
Osterbrock, D. E. 1958, *Publ. A. S. P.*, **70**, 399.
Osterbrock, D. E., and Dufour, R. J. 1973, *Ap. J.*, **185**, 441.
Pradhan, A. K. 1976, *M.N.R.A.S.*, **177**, 31.
Raymond, J. 1976, Ph.D. thesis, University of Wisconsin.
_____. 1979, *Ap. J. Suppl.*, **39**, 1.
Robbins, R. R. 1968, *Ap. J.*, **151**, 511.
Robbins, R. R., Daltabuit, E., and Cox, D. P. 1979, *Ap. J. (Letters)*, **169**, L77.
Salpeter, E. E. 1977, *Ann. Rev. Astr. Ap.*, **15**, 267.
Schild, R. E. 1977, *Ap. J.*, **82**, 337.
Schmidt, G., and Miller, J. S. 1979, *Ap. J. (Letters)*, **234**, L191.
Schwartz, R. D. 1975, *Ap. J.*, **195**, 631.
_____. 1976, *Pub. A. S. P.*, **88**, 159.
Seaton, M. J. 1954, *M.N.R.A.S.* **144**, 154.
Shine, R. A. 1974, Ph.D. thesis, University of Colorado.
Spitzer, L., and Jenkins, E. B. 1975, *Ann. Rev. Astr. Ap.*, **13**, 133.
Strom, S. E., Grasdalen, G. L., and Strom, K. M. 1974, *Ap. J.*, **191**, 111.
Woolley, R. v. d. R., and Stibbs, D. W. N. 1953, *The Outer Layer of a Star* (Oxford: Clarendon Press).

K. H. Böhm, E. W. Brugel, and E. Mannery: Astronomy Department, FM-20, University of Washington, Seattle, WA 98195

© American Astronomical Society • Provided by the NASA Astrophysics Data System